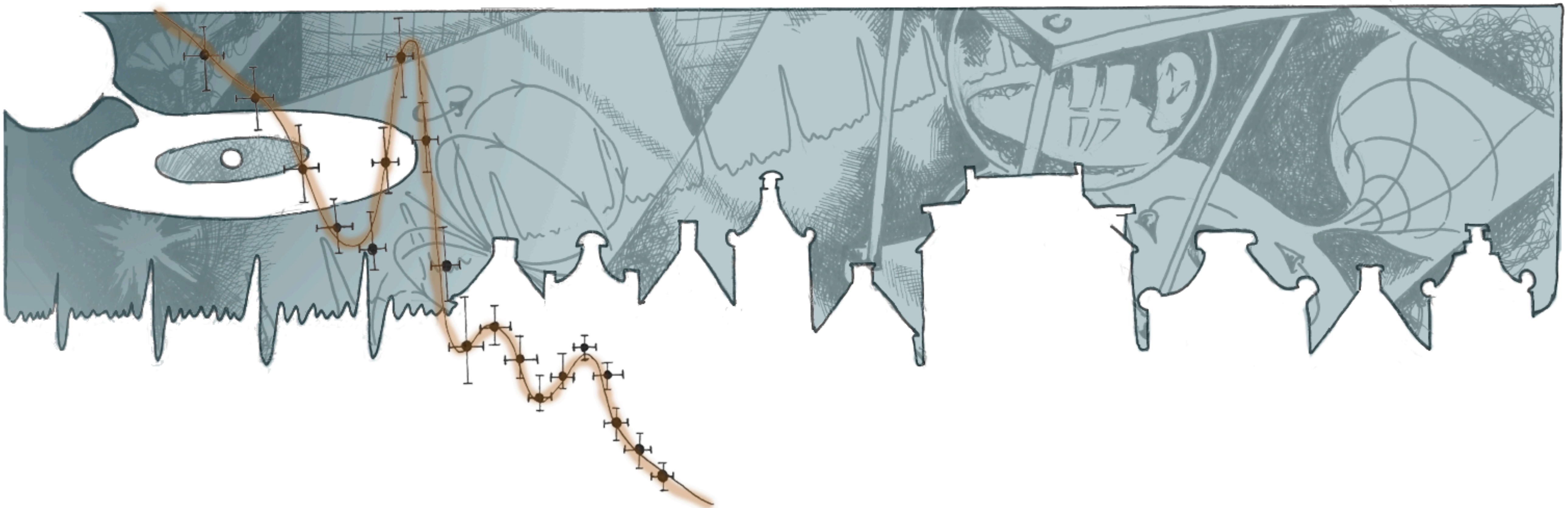

What does the flickering of X-ray pulsar tell us about?

Universiteit Leiden

Netherlands Organisation for Scientific Research

Alexander Mushtukov
Sergey Tsygankov
Juhani Mönkkönen
Galina Lipunova
Adam Ingram
Michiel van der Klis
Simon Portegies Zwart

Black holes

Neutron stars

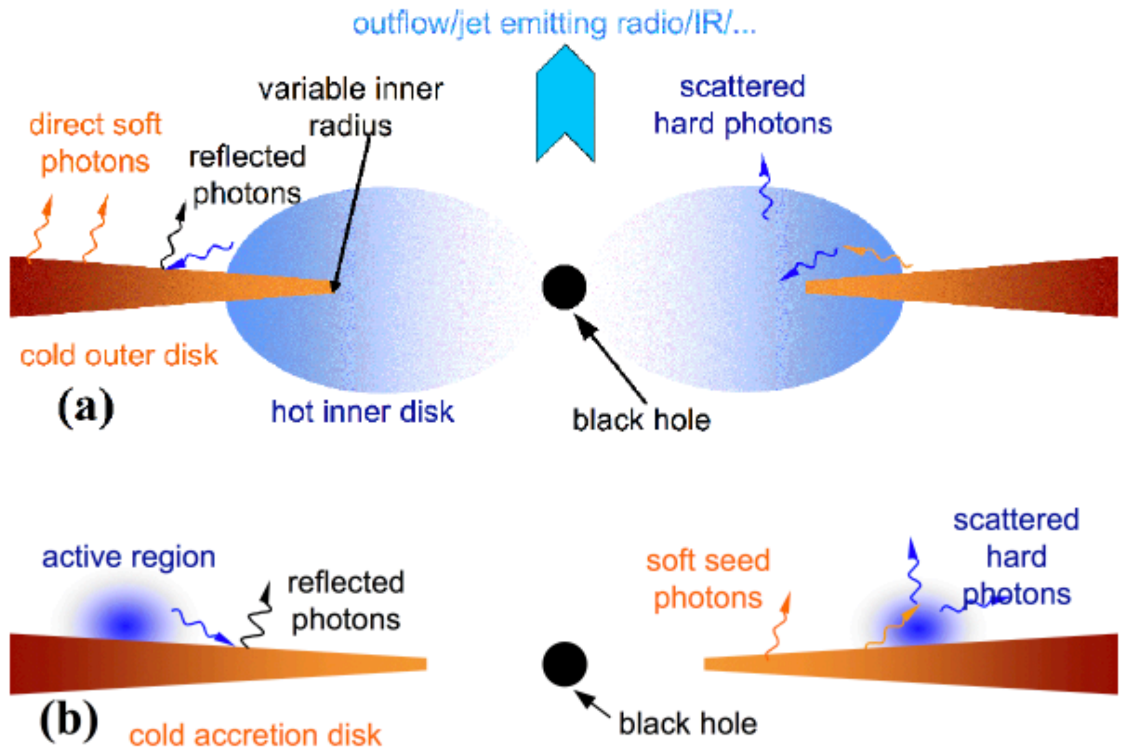

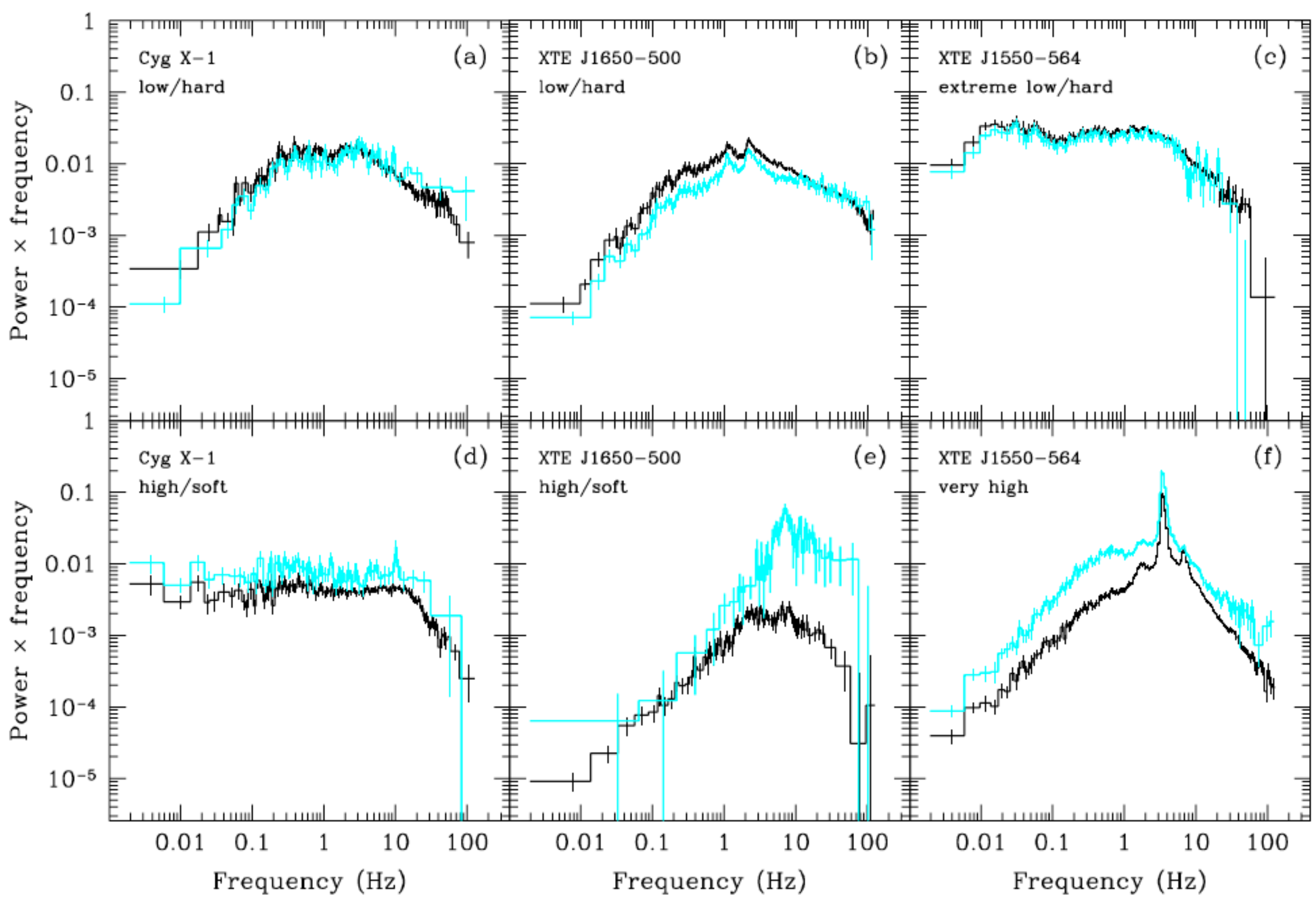

Done & Gierlinski, 2005

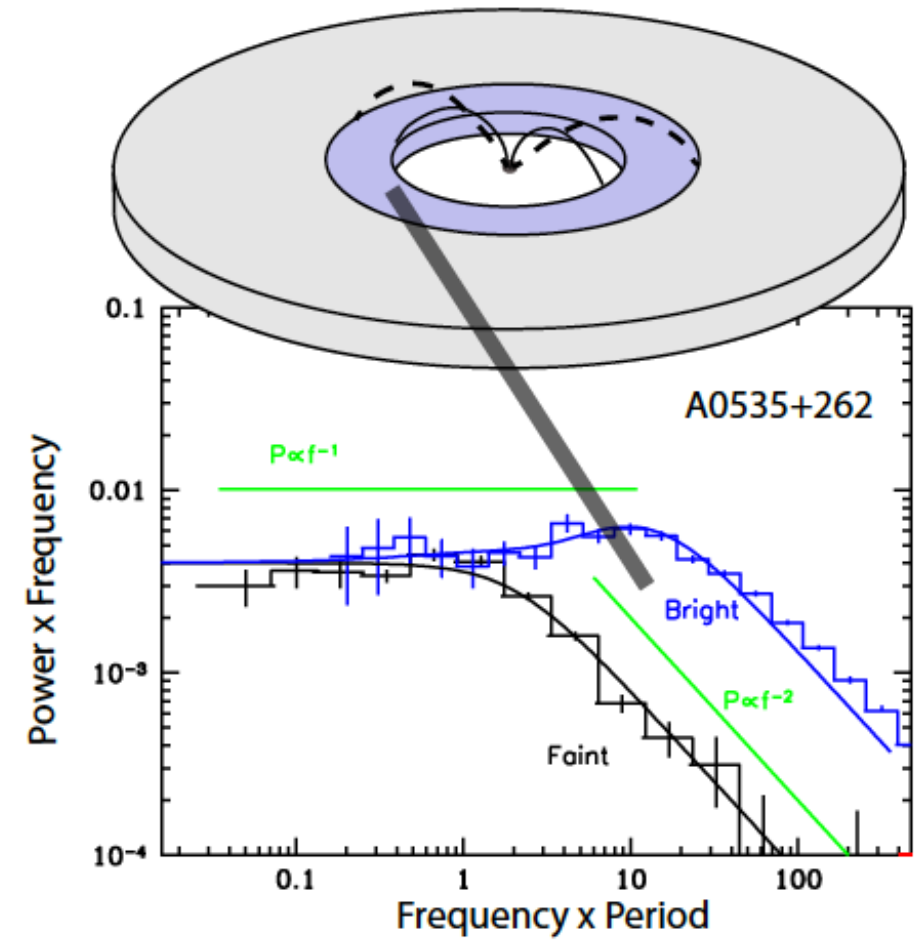

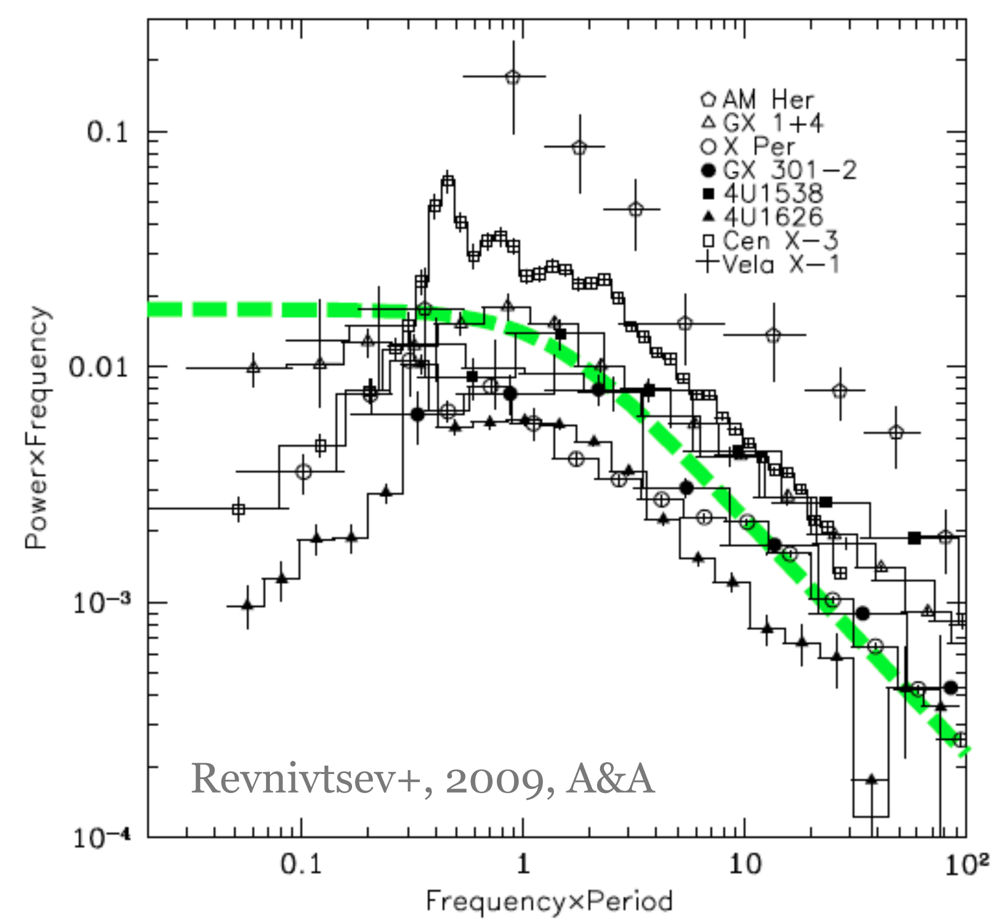

Revnivtsev+, 2009, A&A

X-ray pulsar

Strongly magnetised Neutron Star in binary systems

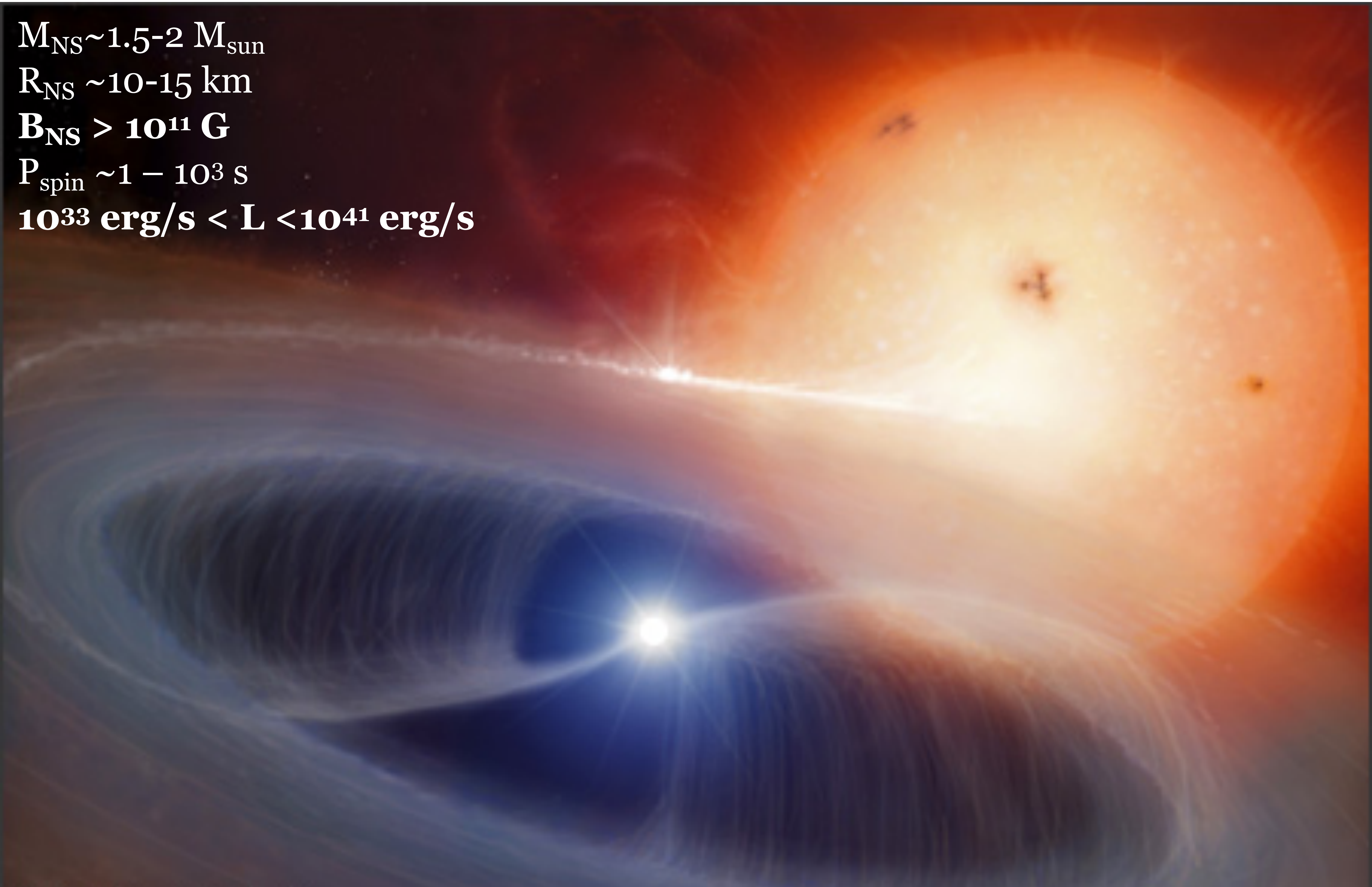

M_{NS}~1.5-2 M_{sun}

R_{NS} ~10-15 km

$B_{NS} > 10^{11}$ G

P_{spin} ~1 – 10^3 s

10^{33} erg/s < L < 10^{41} erg/s

High mass
accretion rate

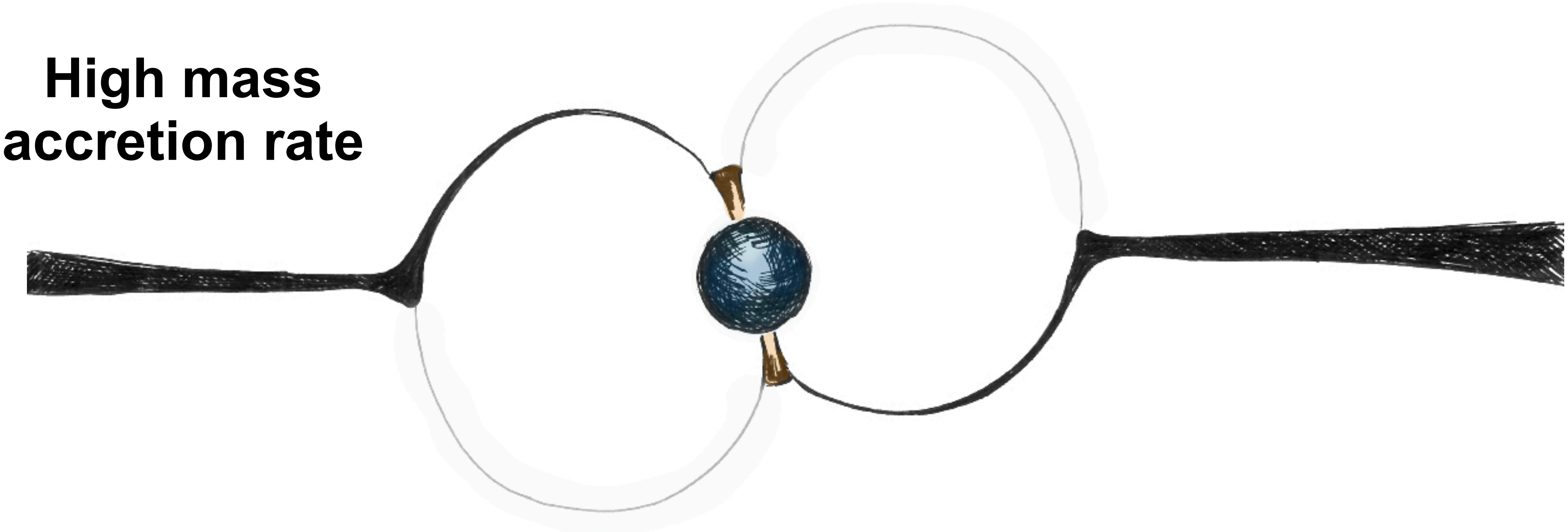

Critical luminosity

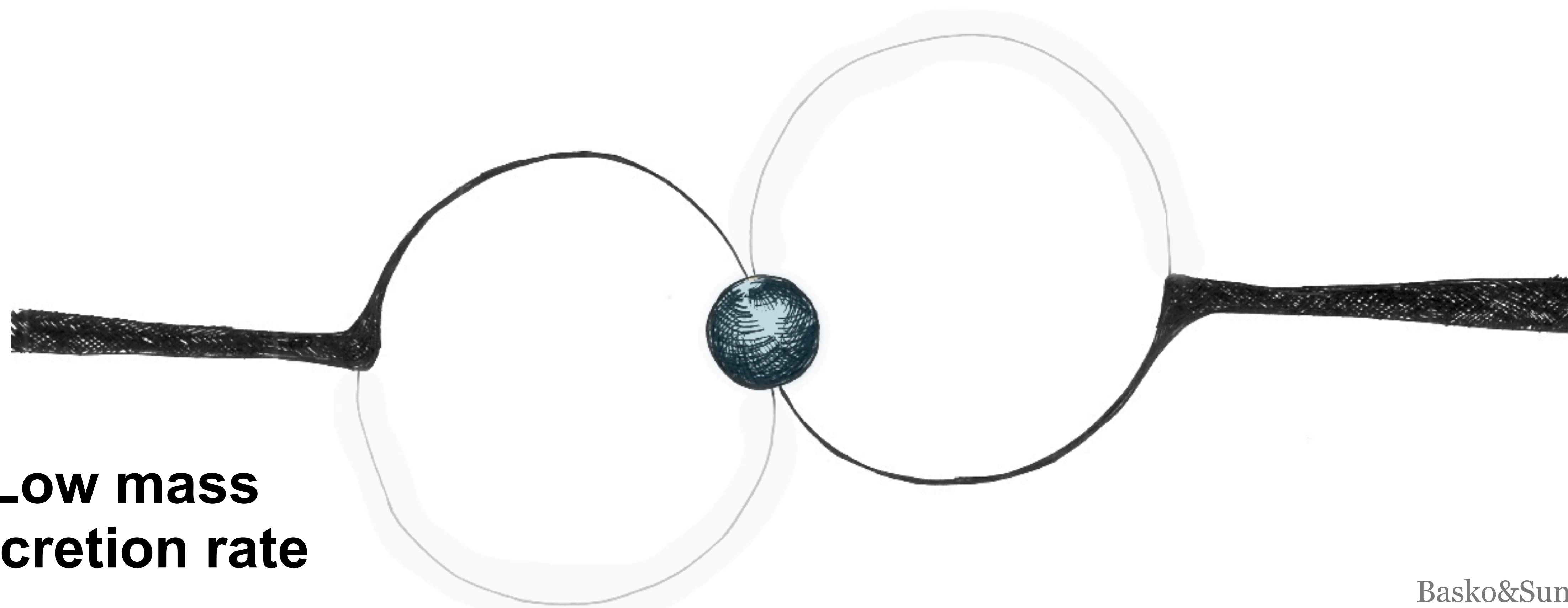

Low mass
accretion rate

Basko&Sunyaev, 1976
AM+, 2015, MNRAS

Propagating fluctuations of the mass accretion rate

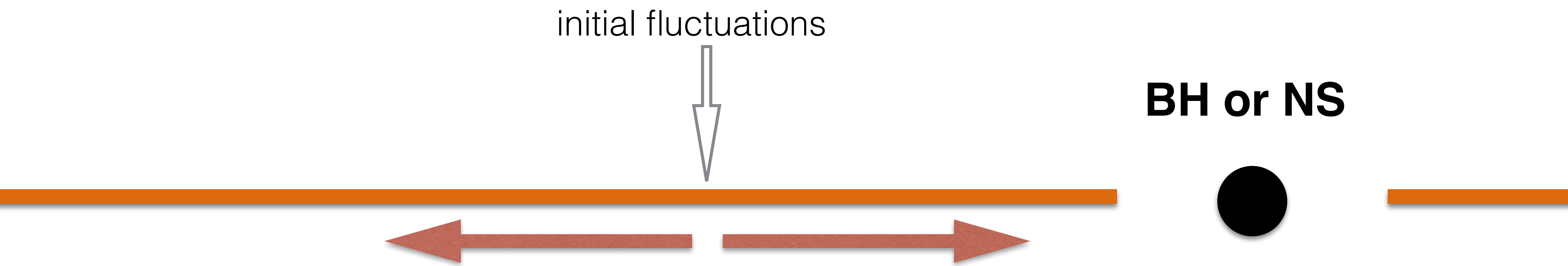

(A)
Initial fluctuations of viscosity in the disc

(B)
Propagation of mass accretion rate fluctuations inside and outside

(C)
Fluctuations of X-ray energy flux:
the mechanisms of conversion is different for BH and NS binaries
In classical XRPs:
the fluctuations of X-ray energy flux replicates fluctuations of the mass accretion rate at the inner disc radius;
accretion discs are geometrically thin in a wide range of accretion luminosity;
We can estimate both inner and outer radii of the disc.

Lyubarskii, 1997, MNRAS
Kotov+, 2001, MNRAS
Ingram & van der Klis, 2013, MNRAS
AM+, 2018, 2019, MNRAS

Propagation of mass accretion rate fluctuations: the basic assumptions

Geometrically thin and **optically thick** accretion disc

Newtonian potential: $\phi_{\rm N} = -\dfrac{GM}{R}$ $\qquad \Omega_{\rm K} = \left(\dfrac{GM}{R^3}\right)^{1/2} = 11.5\left(\dfrac{m}{R_8^3}\right)^{1/2}\ \mathrm{rad\,s^{-1}}$

The equation of viscous diffusion: $\dfrac{\partial \Sigma(R,t)}{\partial t} = \dfrac{1}{R}\dfrac{\partial}{\partial R}\left[R^{1/2}\dfrac{\partial}{\partial R}\left(3\nu\Sigma R^{1/2}\right)\right]$

Kinematic viscosity: $\nu = \dfrac{2}{3}\alpha c_{\rm s} H = \dfrac{2}{3}\dfrac{\alpha c_{\rm s}^2}{\Omega_{\rm K}}$

generally non-linear equation

We are lucky if $\nu = \nu_0 (R/R_0)^n$

$$\frac{\partial \Sigma}{\partial t} = D_{\rm N}(h,M)\frac{\partial^2(h\nu\Sigma)}{\partial h^2}, \quad D_{\rm N}(h,M) = \frac{3}{4}\frac{(GM)^2}{h^3}$$

linear equation

Green's function

Any solution can be represented as

$$\Sigma(R,t) = \int_{R_{\rm in}}^{R_{\rm out}} G(R,R',t-t_0)\Sigma(R',t_0)\mathrm{d}R'$$

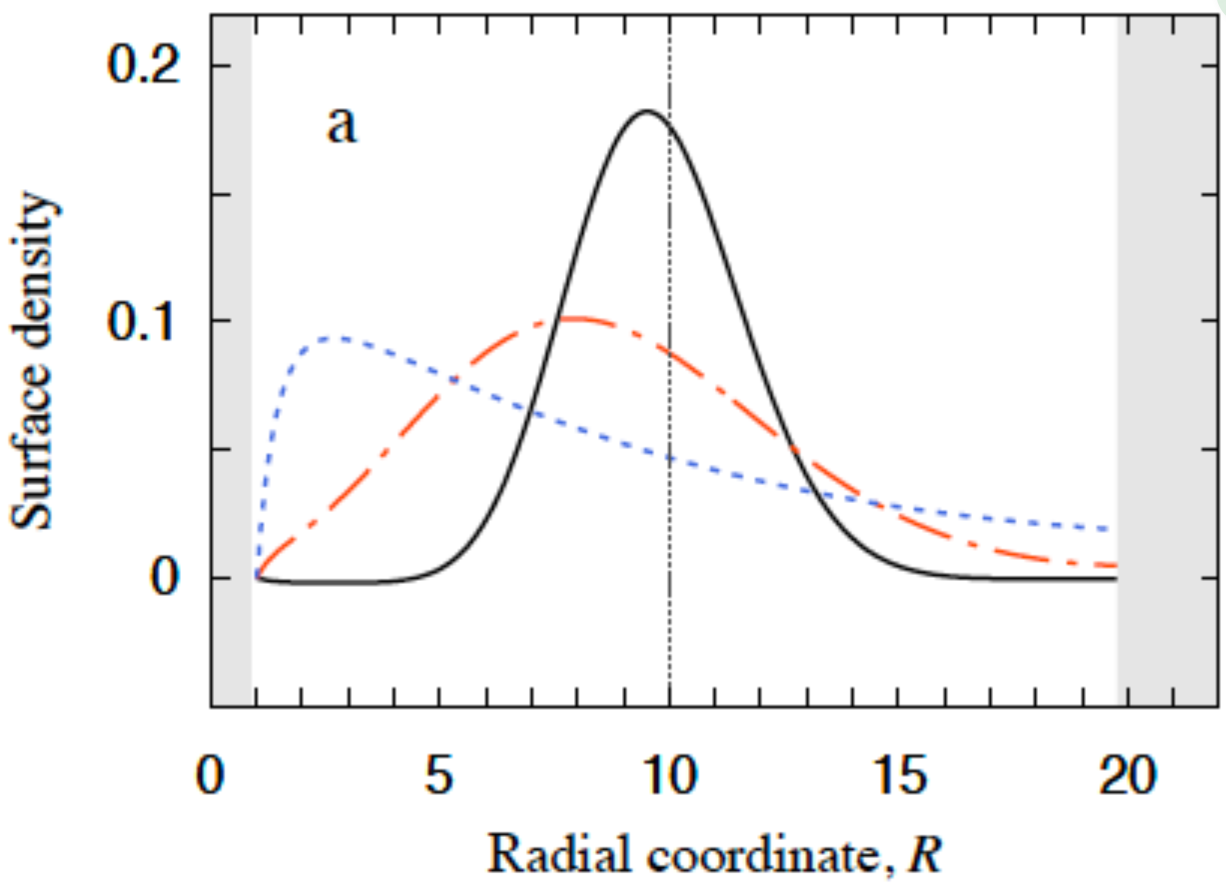

t = 0.04t$_{\rm in}$

t = 0.16t$_{\rm in}$

t = 0.64t$_{\rm in}$

The exact Green's function is defined by viscosity (coefficient n) and boundary conditions.
The exact analytical solutions were found for a few particular cases:

(a) $\mathbf{R_{in}=0, R_{out}=\infty}$ *(Lynden-Bell & Pringle, 1974)*
(b) $\mathbf{R_{in}>0, R_{out}=\infty}$ *(Tanaka, 2011)*
(c) $\mathbf{R_{in}=0, R_{out}<\infty}$ *(Lipunova, 2015)*
(d) $\mathbf{R_{in}>0, R_{out}<\infty}$ *(AM, Lipunova+, 2019)*
(e) $\mathbf{R_{in}=R_{isco}, R_{out}=\infty}$**, GR Green functions** *(Balbus, 2017)*

Green's function

Any solution can be represented as

$$\Sigma(R,t) = \int_{R_{\rm in}}^{R_{\rm out}} G(R,R',t-t_0)\Sigma(R',t_0)\mathrm{d}R'$$

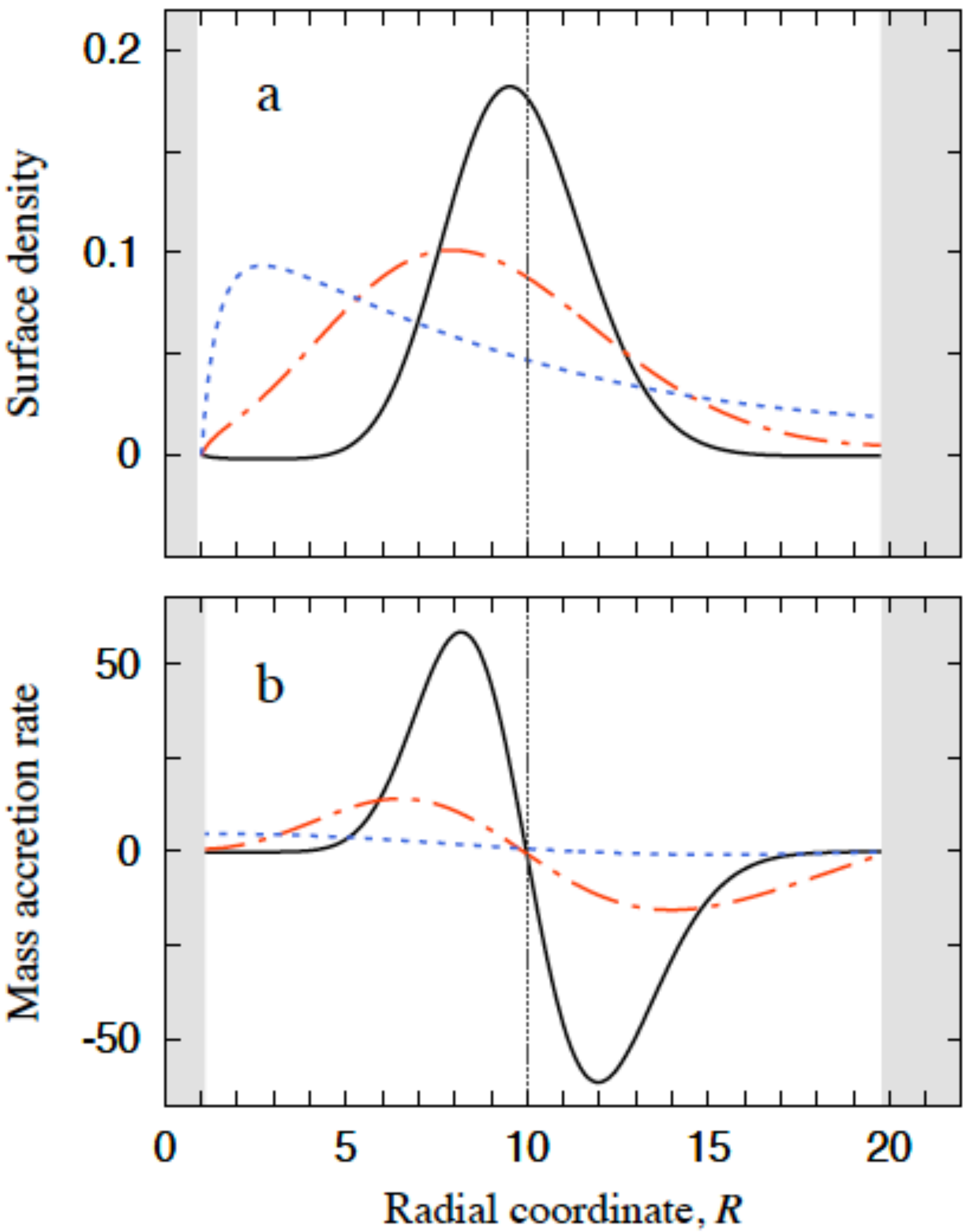

Corresponding mass accretion rate:

$$\dot{M}(R,t) = 6\pi R^{1/2}\frac{\partial}{\partial R}\left(\nu\Sigma(R,t)R^{1/2}\right)$$

Green's function for the mass accretion rate:

$$G_{\dot{M}}(R,R',t) = 6\pi R^{1/2}\frac{\partial}{\partial R}\left(\nu G(R,R',t)R^{1/2}\right)$$

Mass accretion rate fluctuations in the time domain

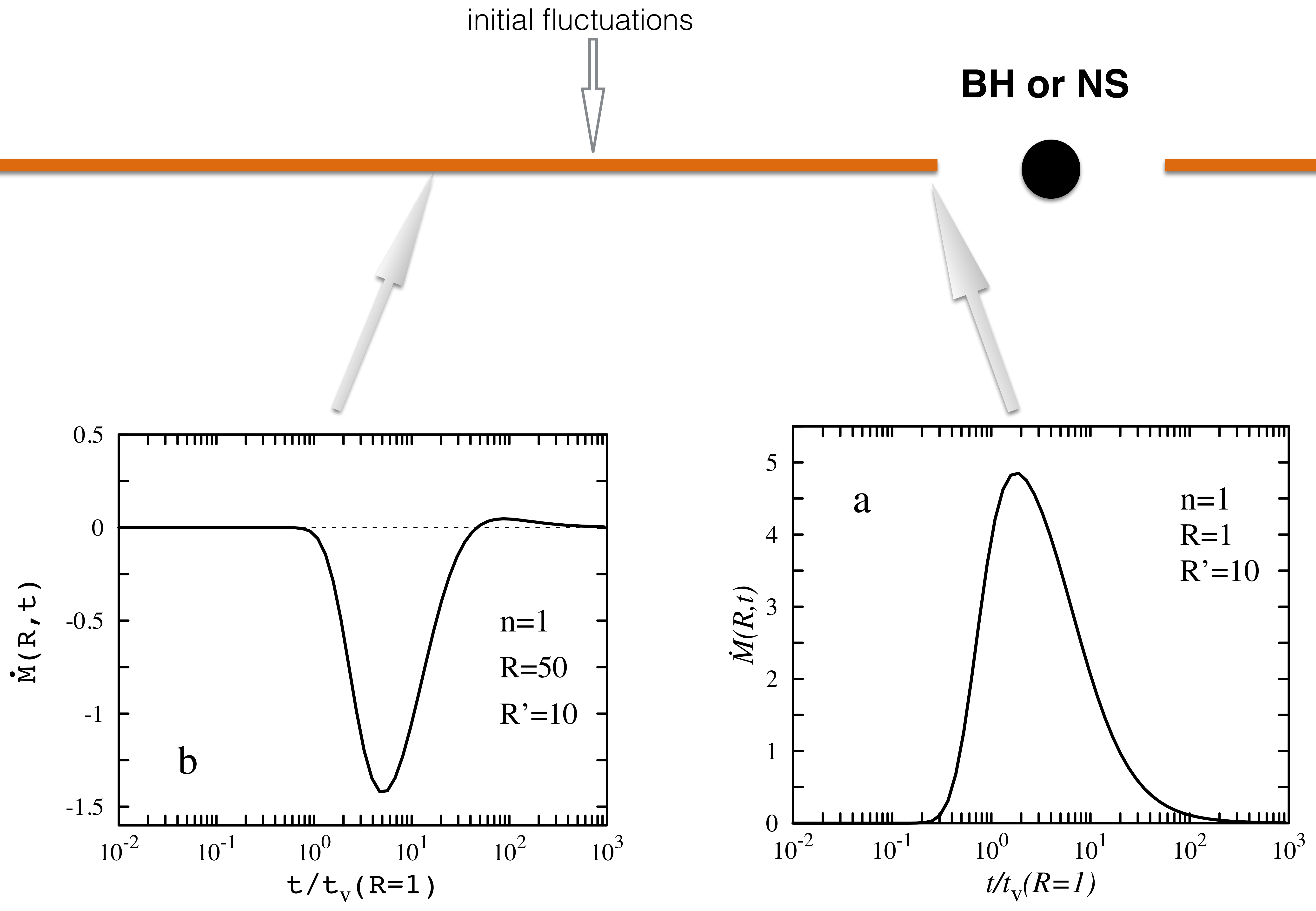

Mass accretion rate fluctuations: the time domain and the frequency domain

$$\dot{m}(R,t) = \int_{R_{\rm in}}^{R_{\rm out}} \mathrm{d}R'\, G_{\dot{M}}(R,R',t) \otimes_t \frac{a(R',t)}{R'}$$

Fourier transform

$$\overline{\dot{m}}(R,f) = \int_{R_{\rm in}}^{R_{\rm out}} \mathrm{d}R'\, \overline{G}_{\dot{M}}(R,R',f)\overline{A}(R',f)$$

We need to construct Green's functions in the frequency domain.
The Green's functions play a role of the transfer functions in the f-domain.

Mass accretion rate fluctuations in the frequency domain

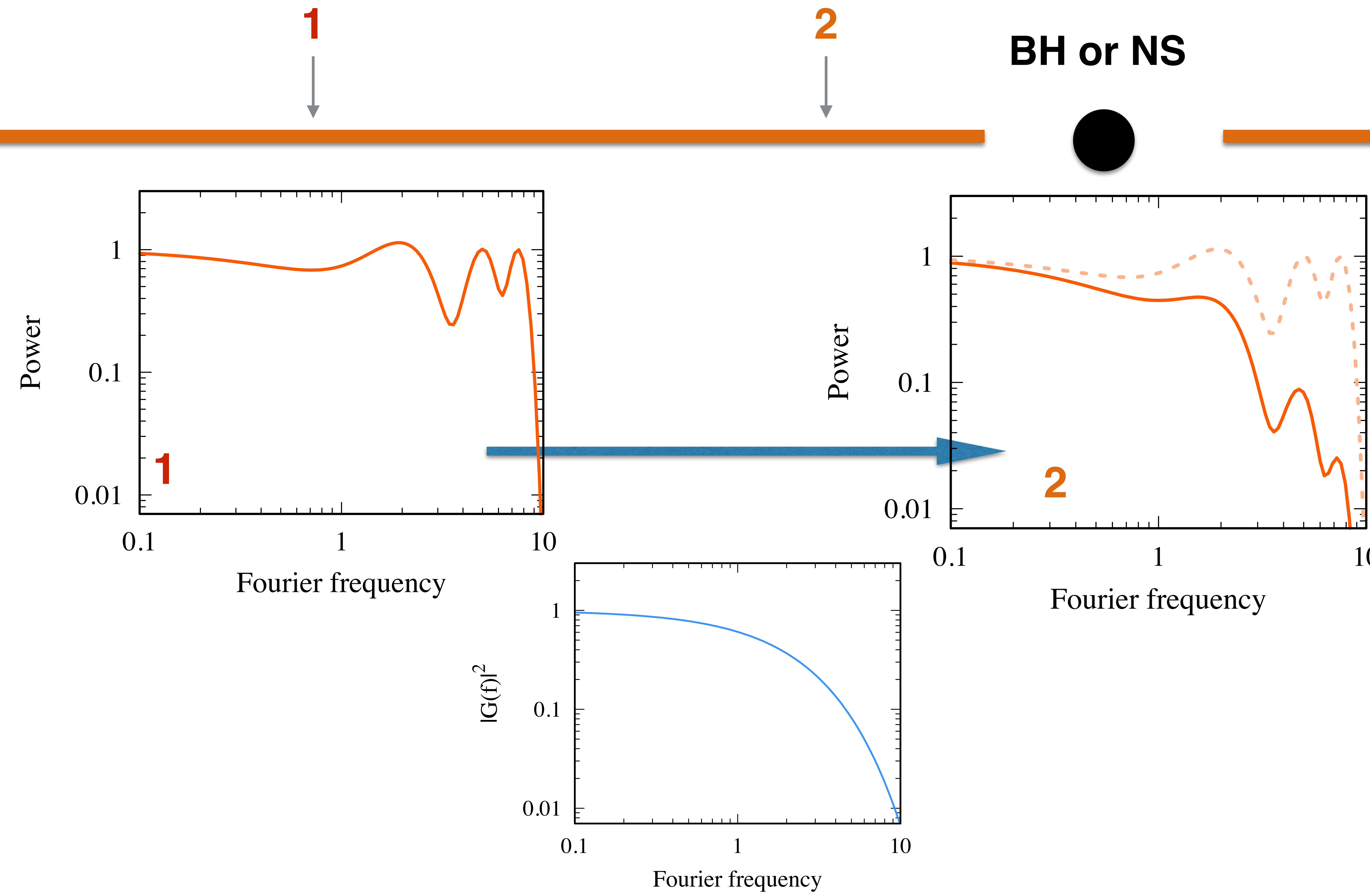

Mass accretion rate fluctuations in the frequency domain

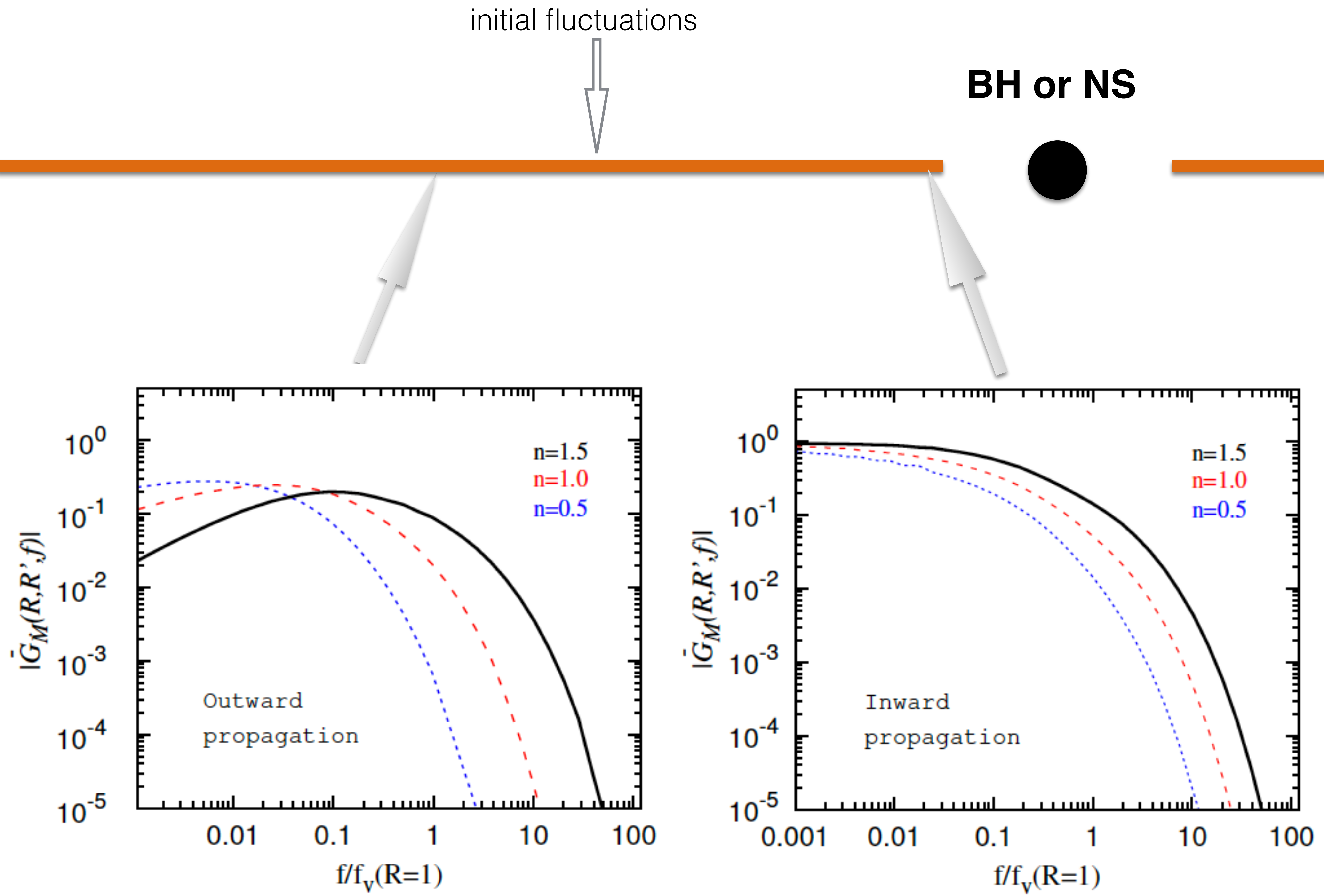

Aperiodic variability in X-ray Pulsars

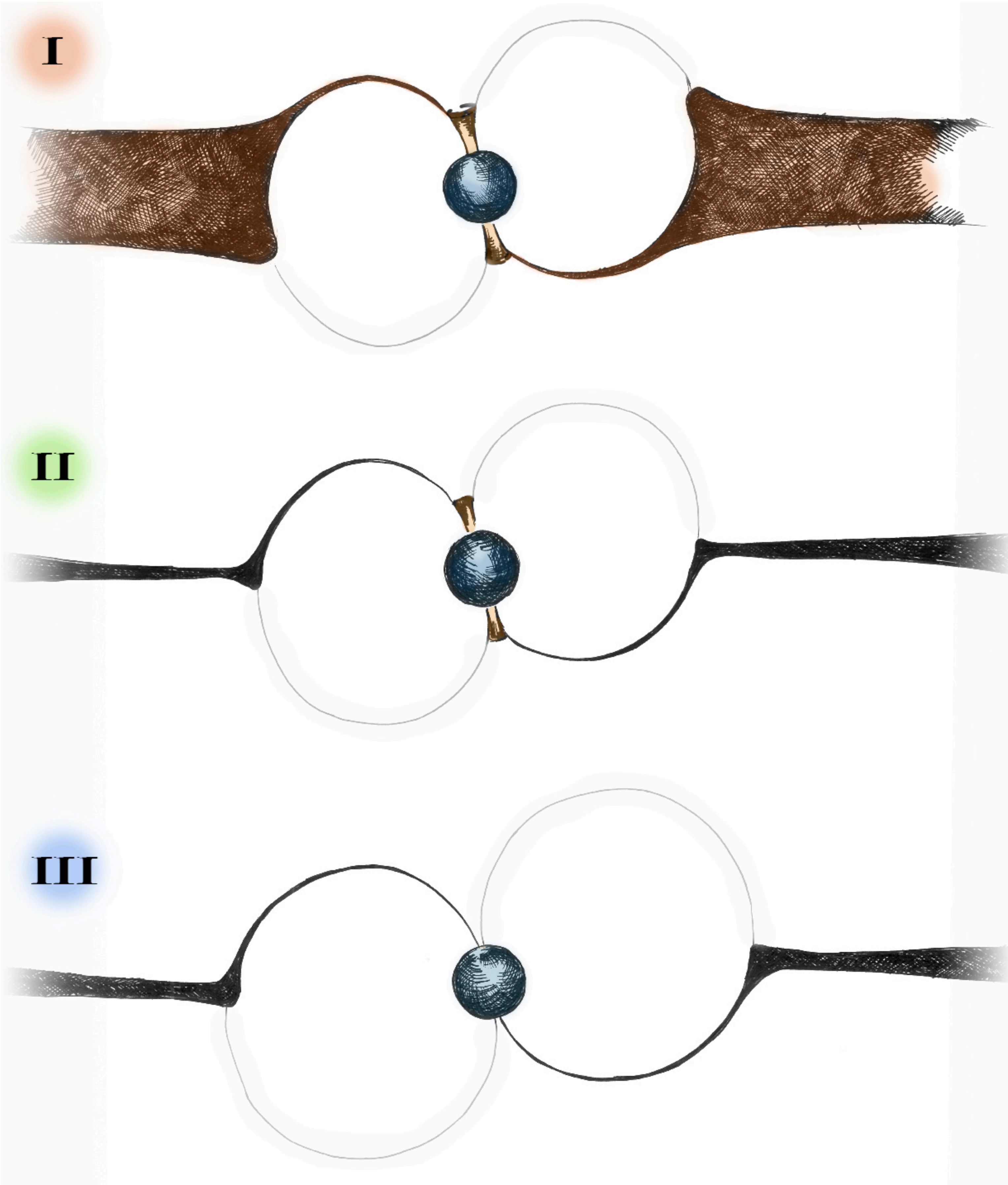

Accretion disc does not contribute significantly to X-ray energy flux

Mass accretion rate fluctuations at the NS surface replicate the fluctuations at the inner disc radius

Observed fluctuations of X-ray energy flux can be affected by variability in geometry of the emitting region

Typical Power Density Spectra

The main parameters:

R_{in} & *R_{out}*

n

PDS of initial fluctuations

$$R_{\rm in} \approx R_{\rm m} \simeq 2.4\times10^{8}\,\Lambda B_{12}^{4/7} L_{37}^{-2/7} m^{1/7}\ {\rm cm}$$

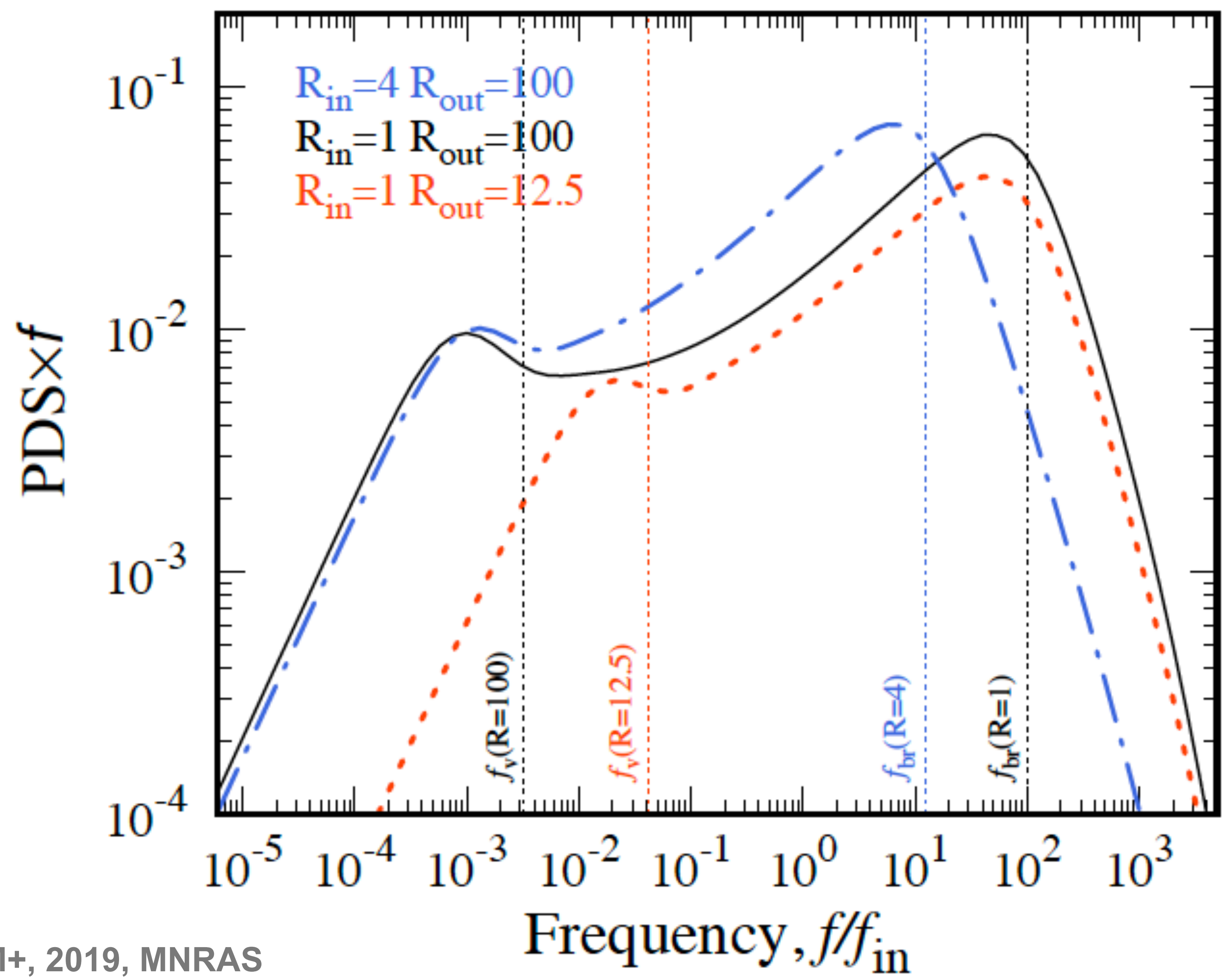

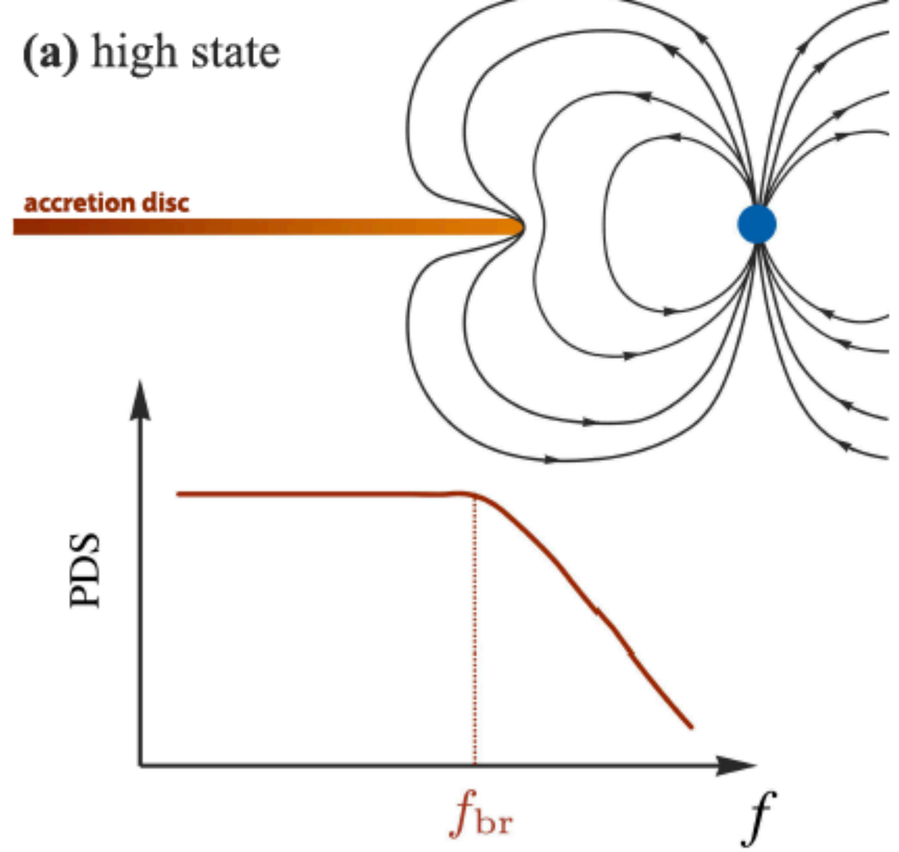

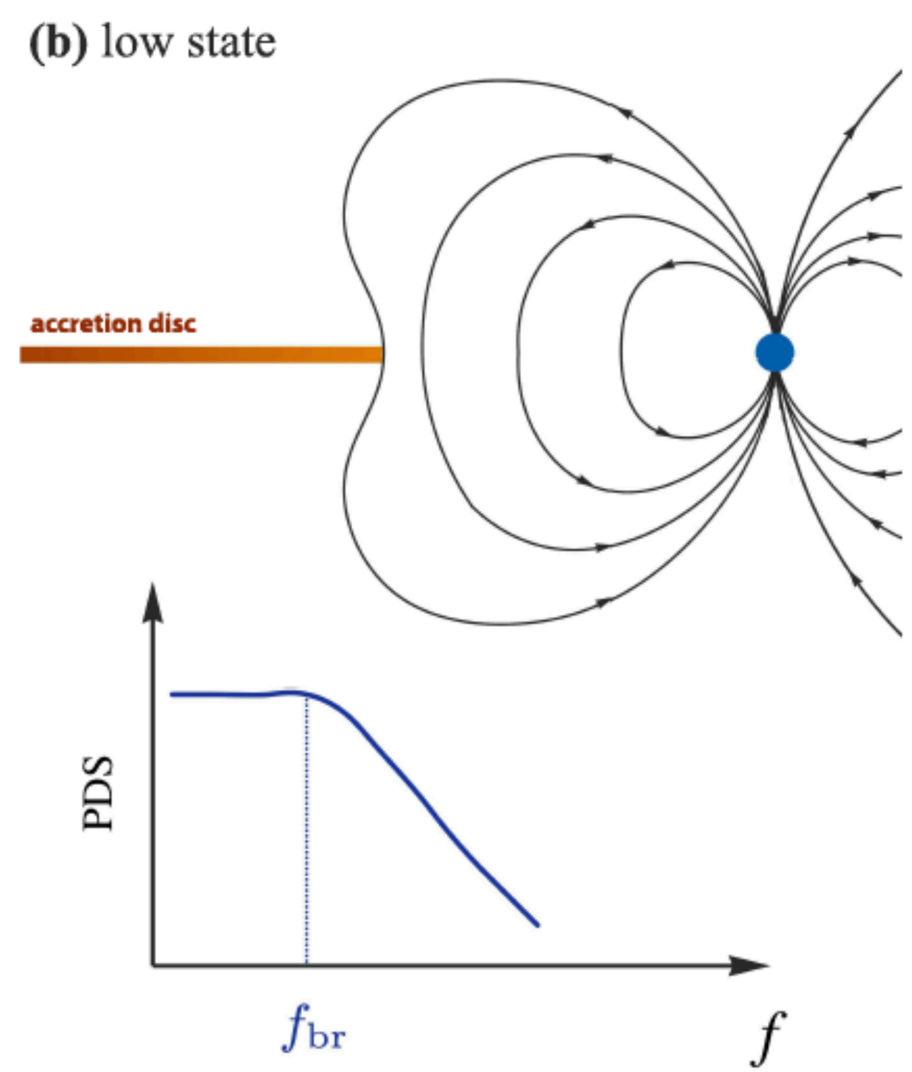

AM+, 2019, MNRAS

X-ray pulsar A0535+26

$E_{cyc,0} \sim 45$ keV $E_{cyc,1} \sim 100$ keV

$P_{spin} \sim 100$ sec

Two luminosity states: $L_1 = 1.7\times10^{35}$ erg/s $L_2 = 3.8\times10^{36}$ erg/s

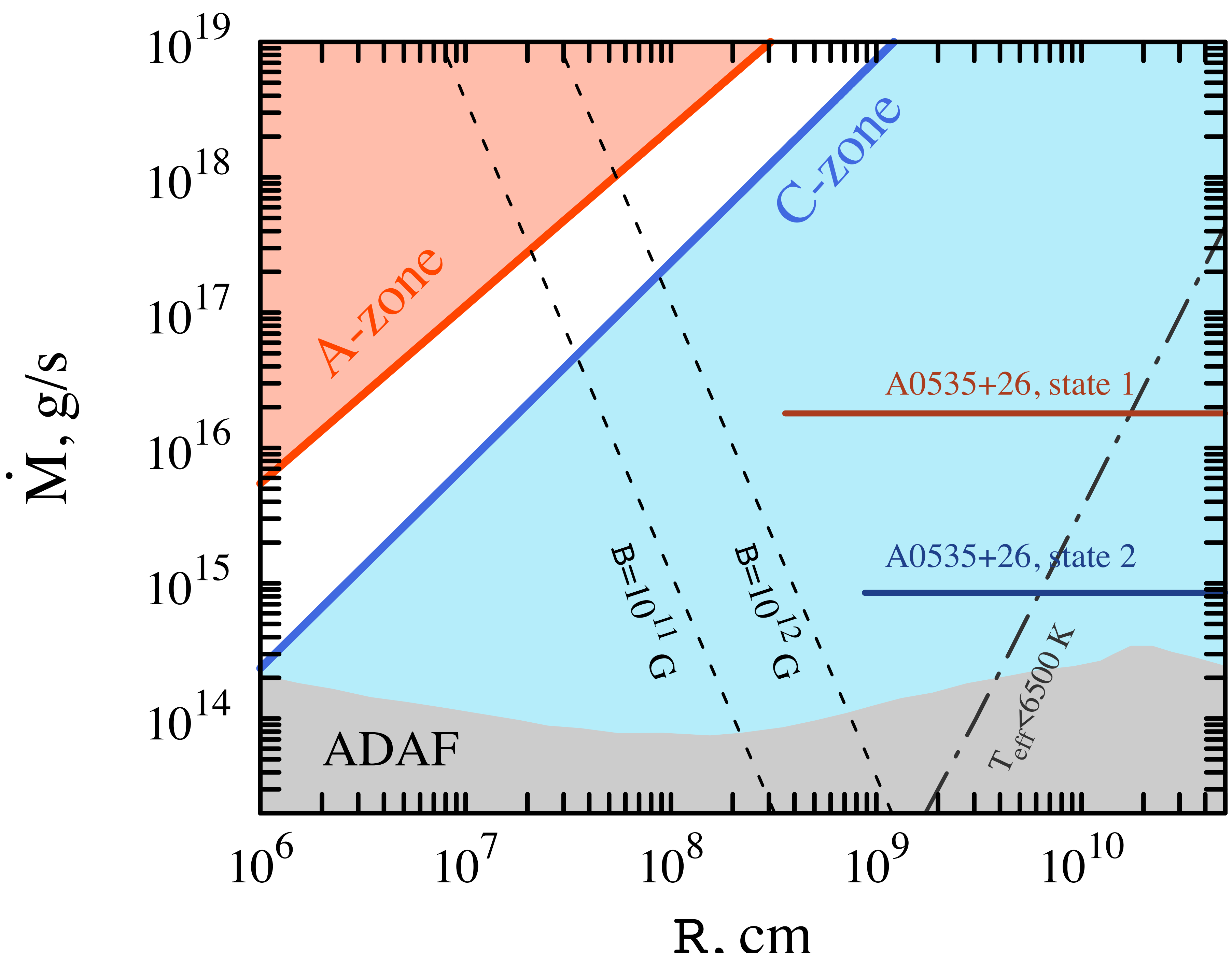

Gas pressure dominated disc

The inner disc is still ionized

Hot spots on the surface ($L_{crit} > 10^{37}$ erg/s)

AM+, 2019, MNRAS

X-ray pulsar A0535+26

$E_{cyc,0} \sim 45$ keV $E_{cyc,1} \sim 100$ keV

$P_{spin} \sim 100$ sec

Two luminosity states: $L_1 = 1.7\times10^{35}$ erg/s $L_2 = 3.8\times10^{36}$ erg/s

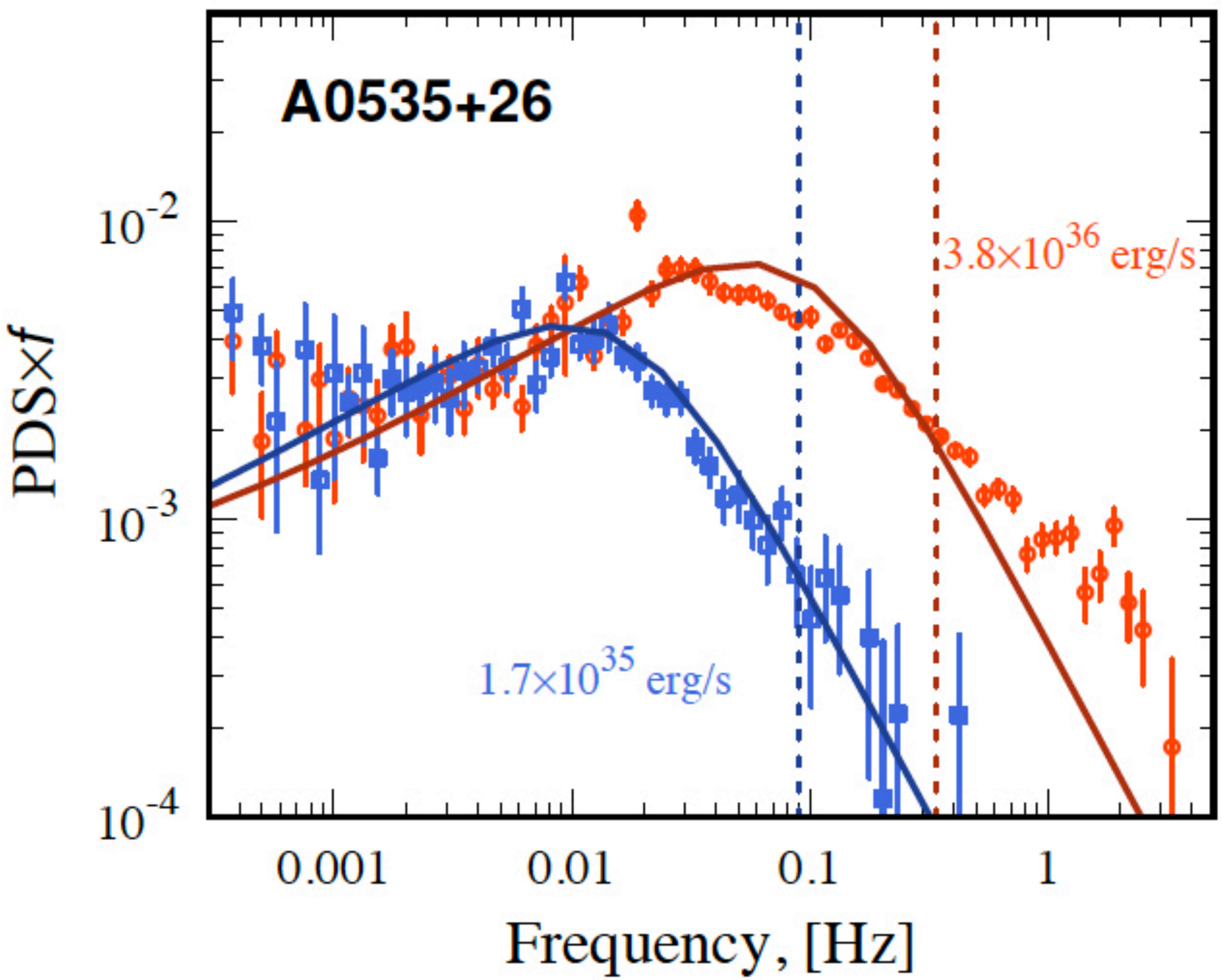

AM+, 2019, MNRAS

X-ray pulsar A0535+26

$E_{cyc,0} \sim 45$ keV $E_{cyc,1} \sim 100$ keV

$P_{spin} \sim 100$ sec

Two luminosity states: $L_1 = 1.7\times10^{35}$ erg/s $L_2 = 3.8\times10^{36}$ erg/s

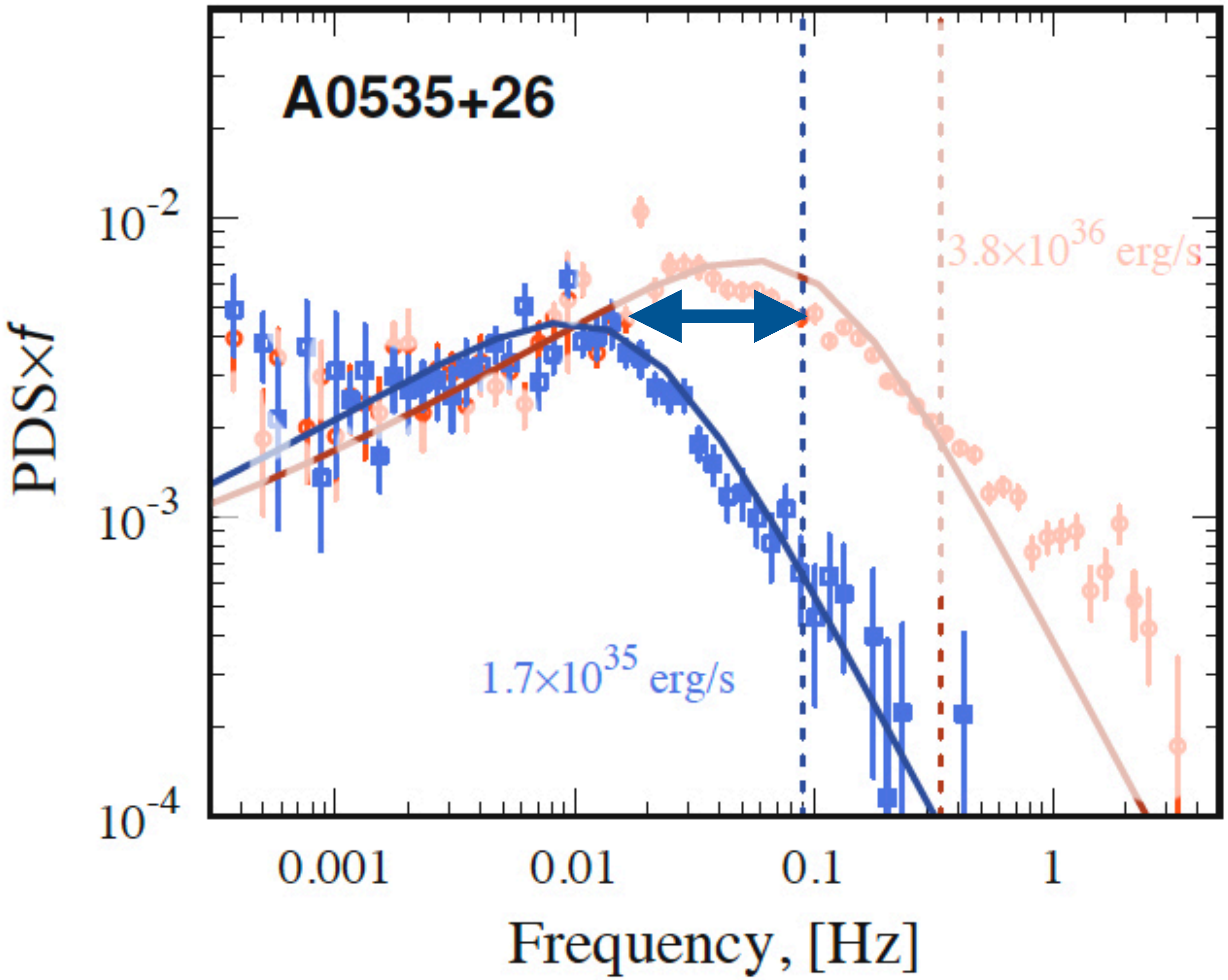

AM+, 2019, MNRAS

X-ray pulsar A0535+26

$E_{cyc,0} \sim 45$ keV $\quad E_{cyc,1} \sim 100$ keV

$P_{spin} \sim 100$ sec

Two luminosity states: $L_1 = 1.7\times10^{35}$ erg/s $\quad L_2 = 3.8\times10^{36}$ erg/s

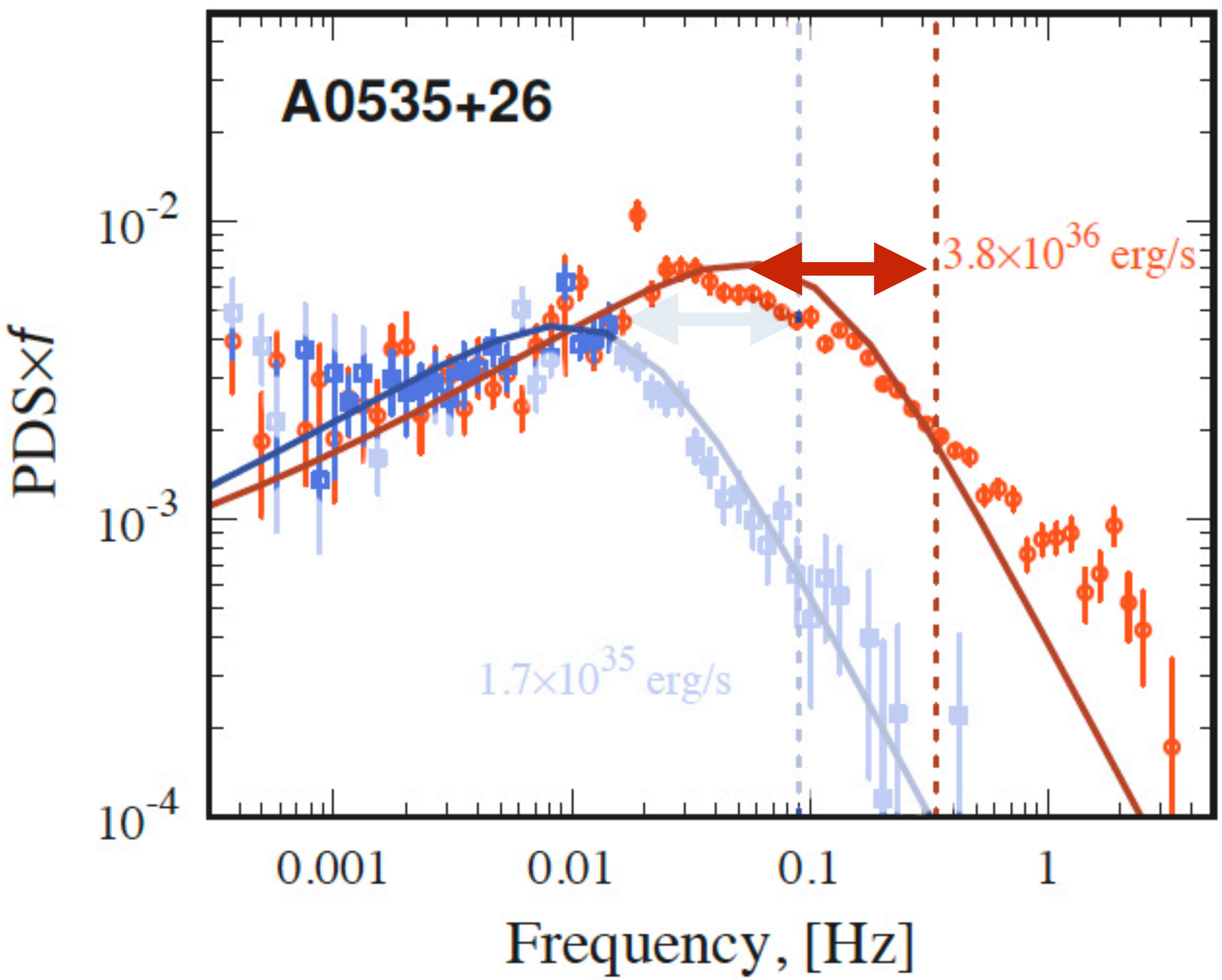

AM+, 2019, MNRAS

X-ray pulsar V 0332+53

$E_{cyc,0} \sim 30$ keV $E_{cyc,1} \sim 60$ keV

$P_{spin} \sim 4.4$ sec

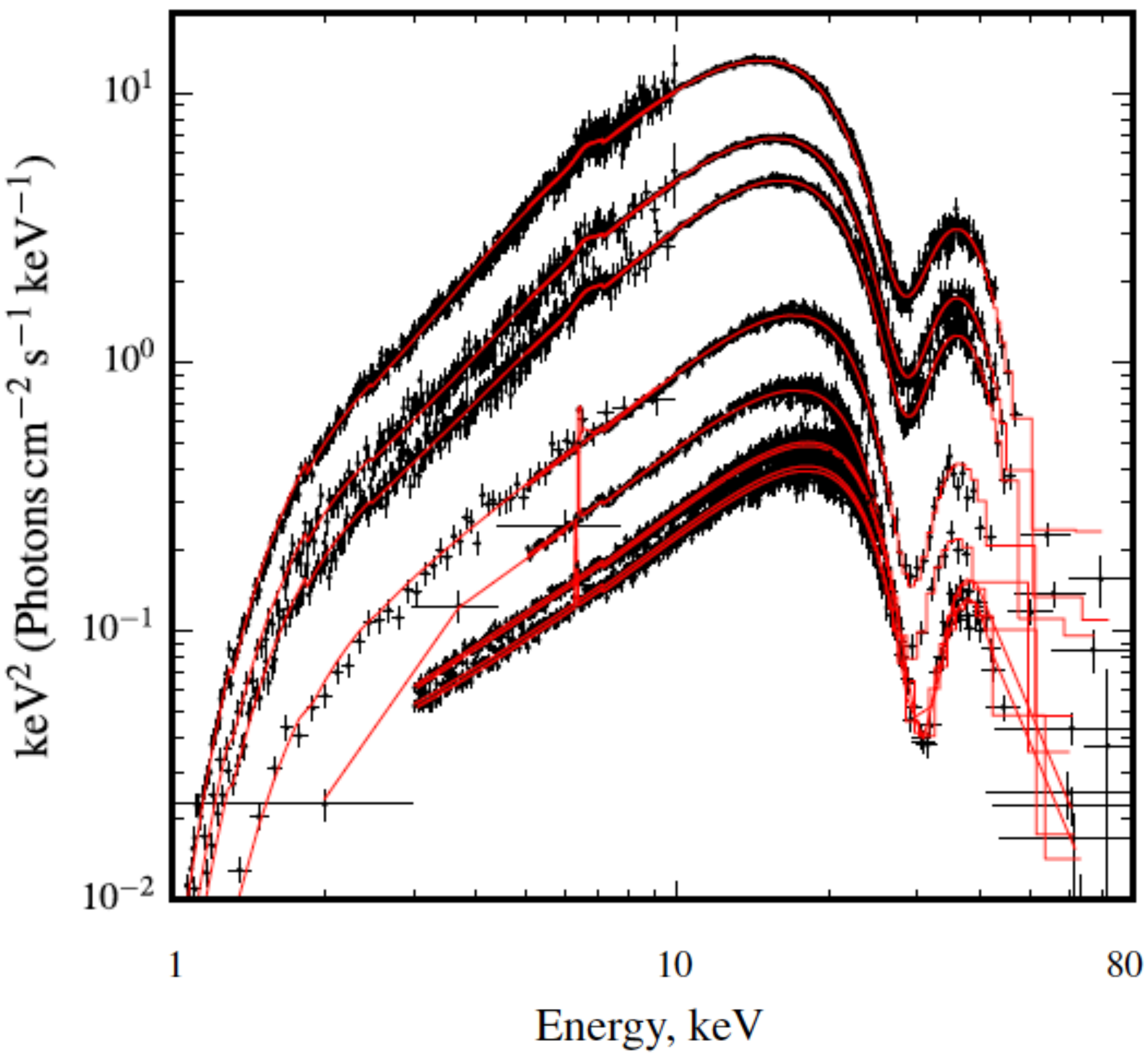

Doroshenko+, MNRAS, 2017

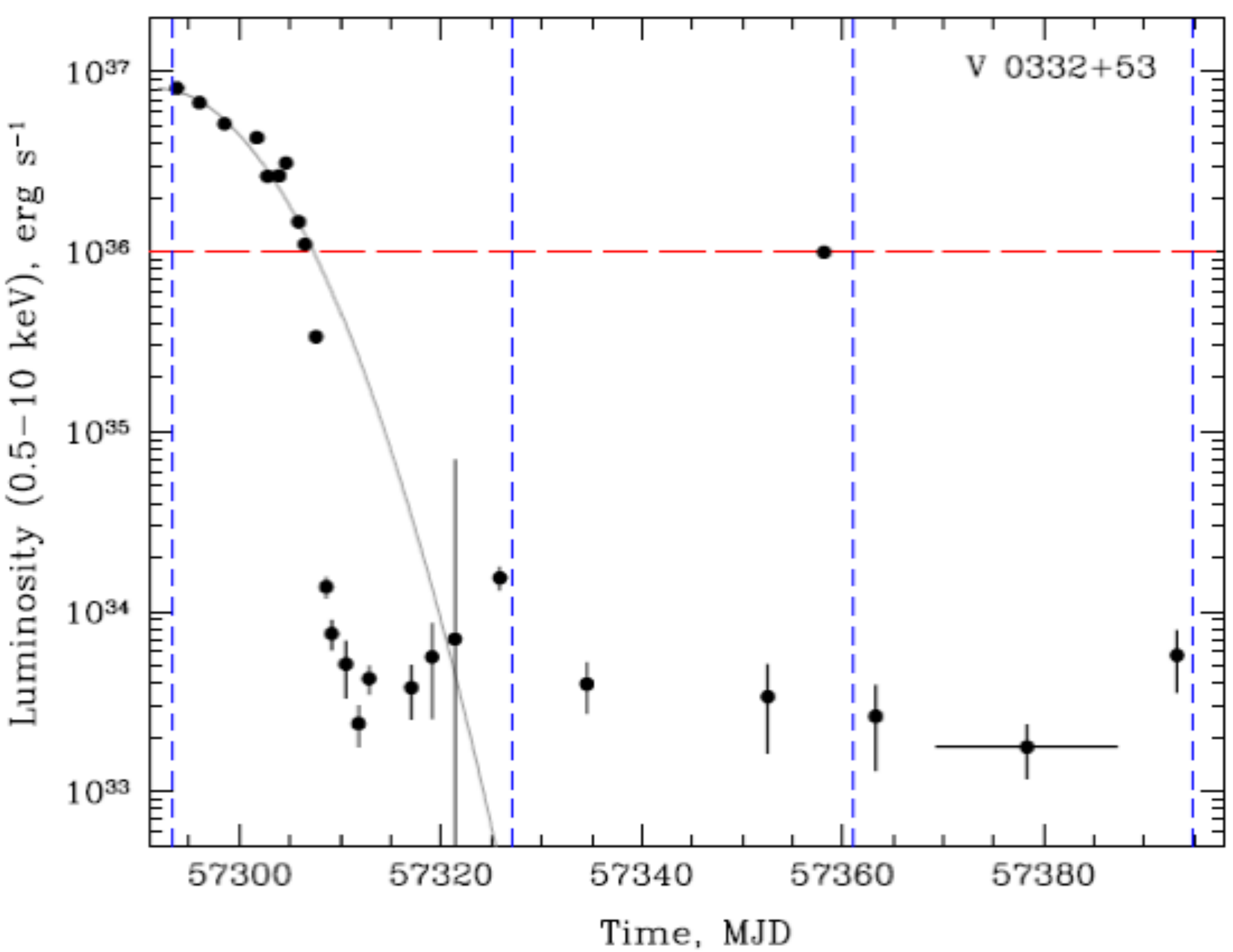

Tsygankov+, A&A, 2016

X-ray pulsar V 0332+53

$E_{cyc,0} \sim 30$ keV $E_{cyc,1} \sim 60$ keV

$P_{spin} \sim 4.4$ sec

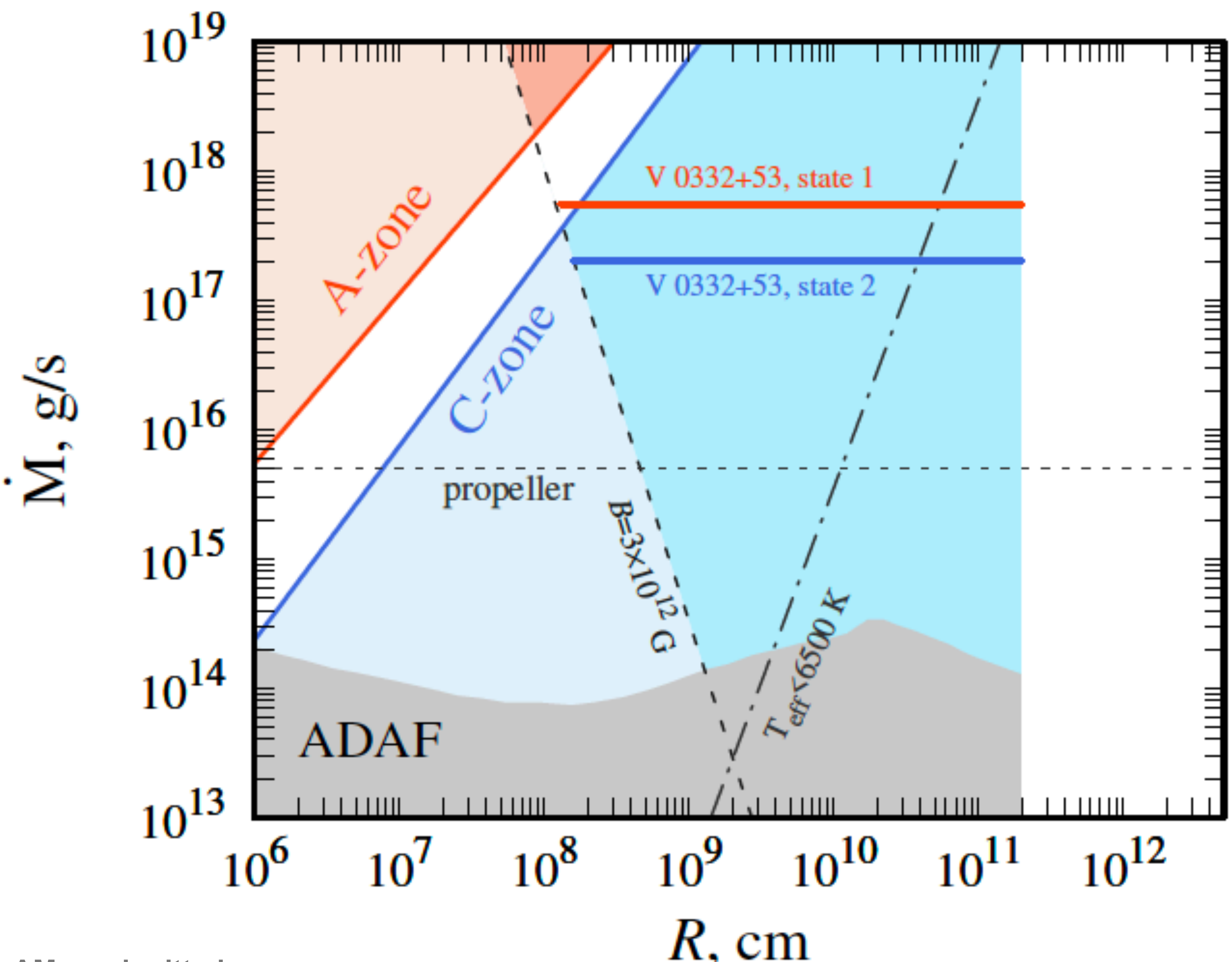

$a > 2.3\times10^{12}$ cm

$e \sim 0.37$

$M < (8\text{-}50)\ M_{sun}$

$R_{out} > 2\times10^{11}$ cm

AM+, submitted

X-ray pulsar V 0332+53

$E_{cyc,0} \sim 30$ keV $E_{cyc,1} \sim 60$ keV

$P_{spin} \sim 4.4$ sec

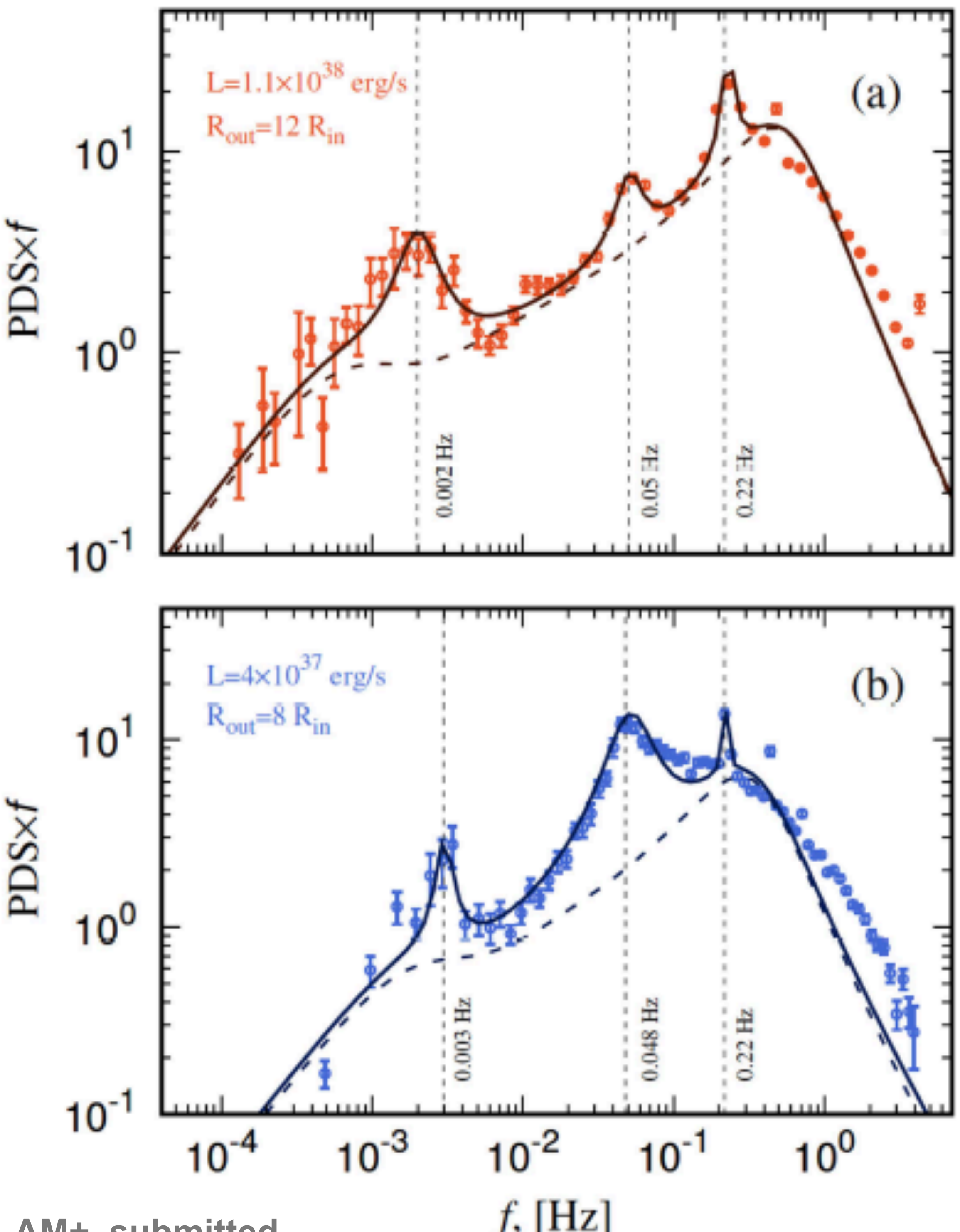

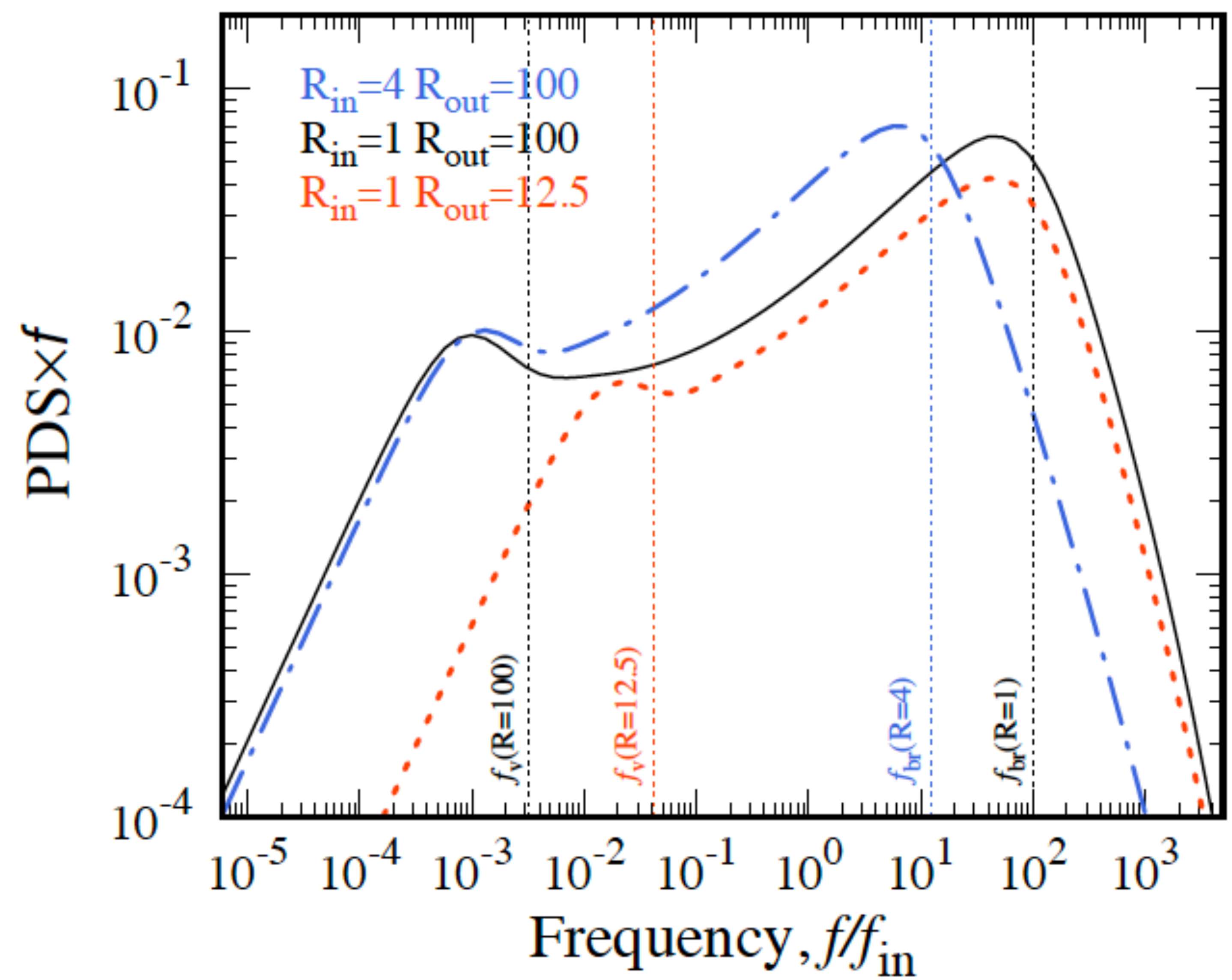

AM+, submitted

X-ray pulsar V 0332+53

$E_{cyc,0} \sim 30$ keV $E_{cyc,1} \sim 60$ keV

$P_{spin} \sim 4.4$ sec

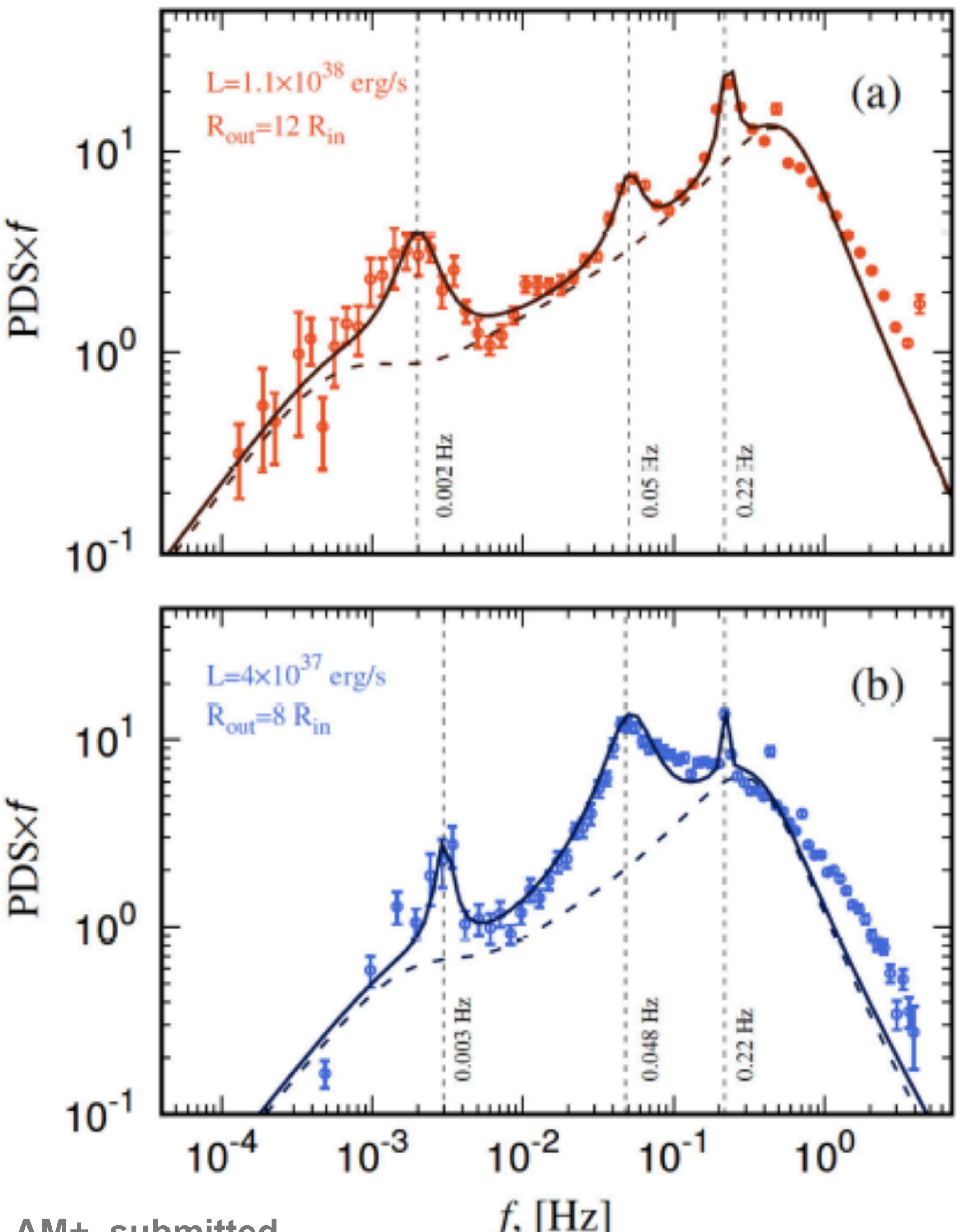

Parameter	High state	Low state
L, erg s^{-1}	1.1×10^{38}	4×10^{37}
$R_{\rm in}$, cm	1.2×10^{8}	1.6×10^{8}
$R_{\rm out}^{\rm (eff)}$, cm	2.4×10^{9}	1.7×10^{9}
f_1, Hz	0.22	0.22
δf_1, Hz	2×10^{-2}	10^{-2}
rms$_1$, %	5.8	2.2
f_2, Hz	5×10^{-2}	4.8×10^{-2}
δf_2, Hz	1.1×10^{-2}	2×10^{-2}
rms$_2$, %	4.2	9
f_3, Hz	2×10^{-3}	3×10^{-3}
δf_3, Hz	8×10^{-4}	4×10^{-4}
rms$_3$, %	5.2	2.2

AM+, submitted

X-ray pulsar V 0332+53

$E_{cyc,0} \sim 30$ keV $E_{cyc,1} \sim 60$ keV

$P_{spin} \sim 4.4$ sec

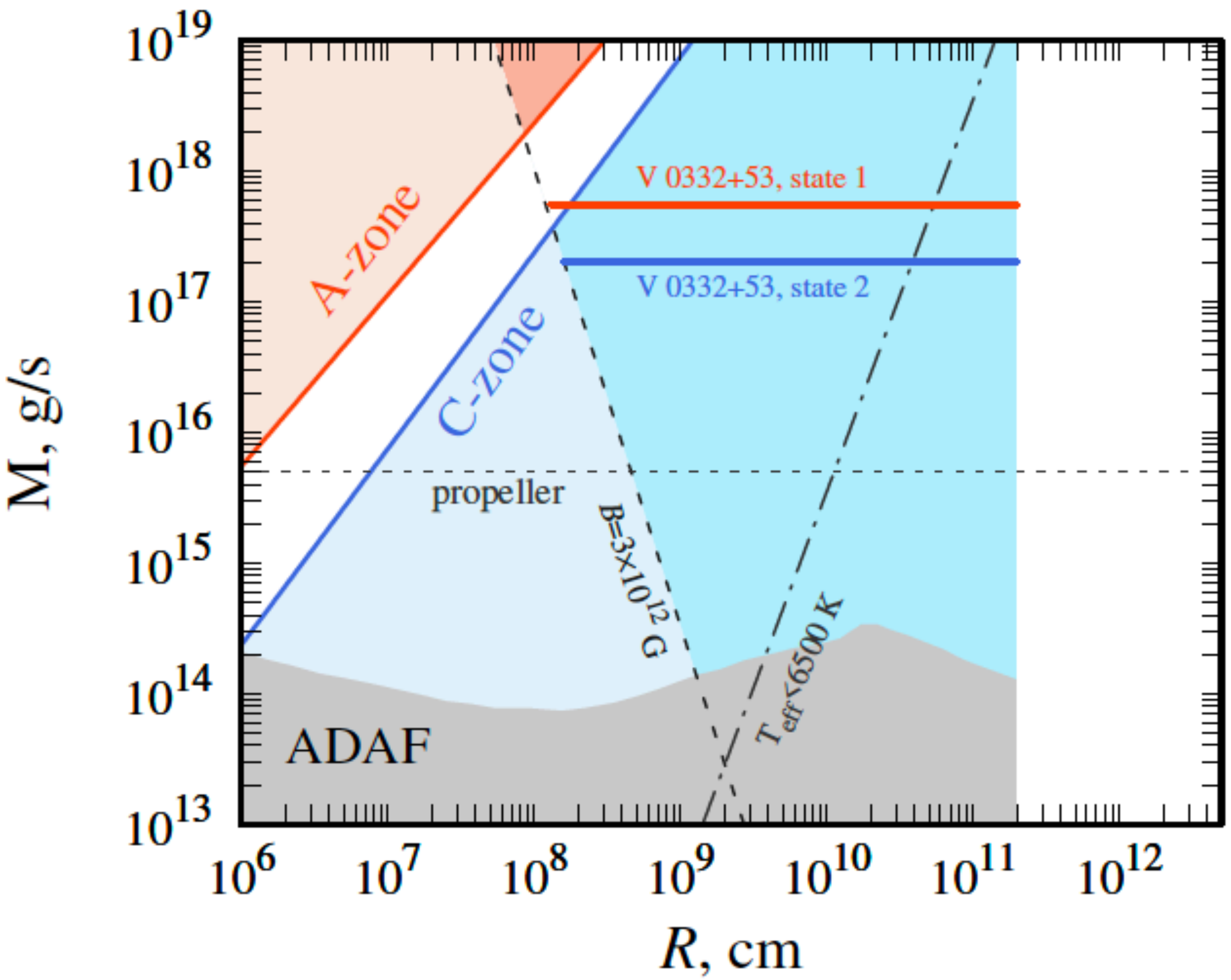

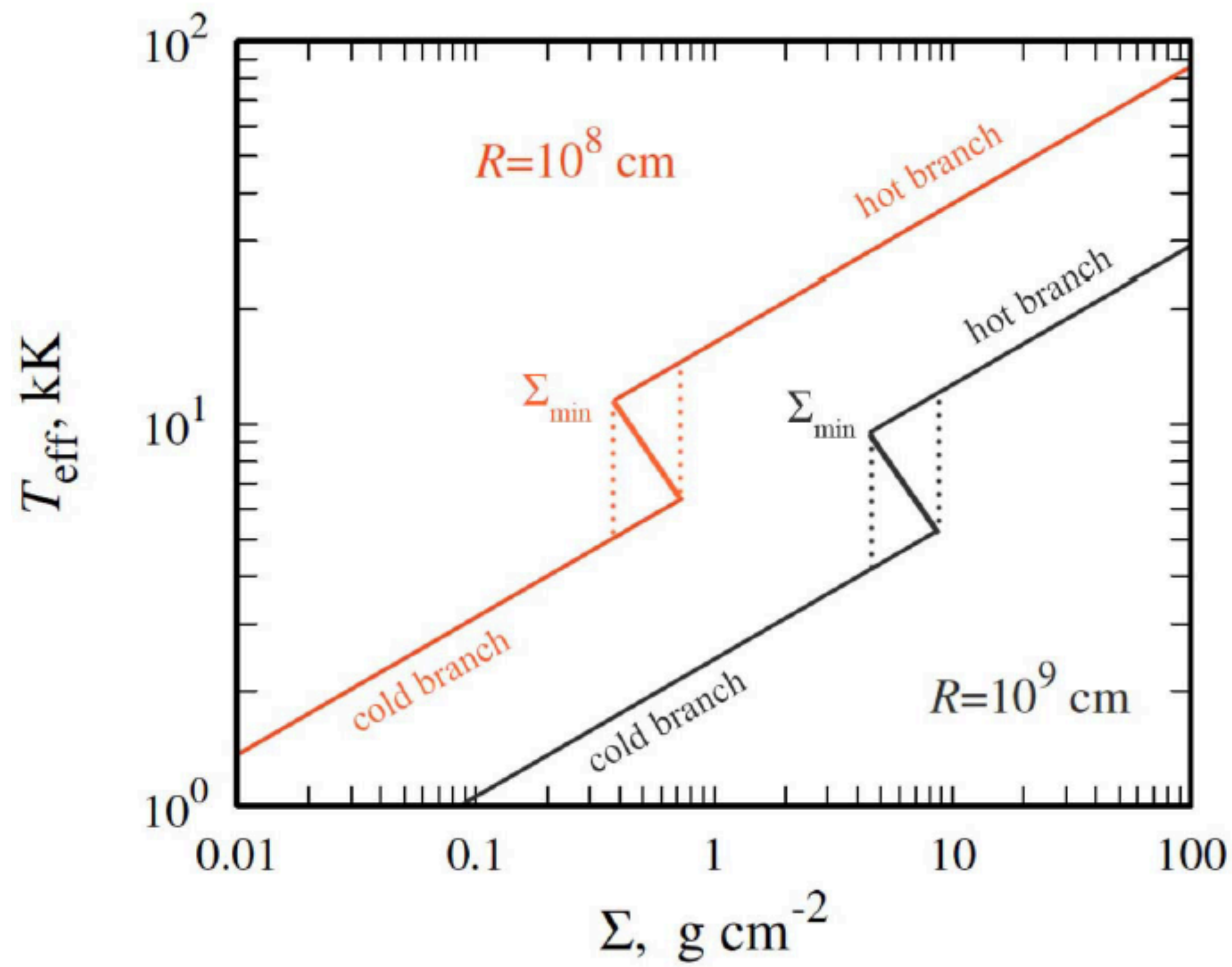

AM+, submitted

Smak, 1984
Cannizzo & Kenyon, 1987

X-ray pulsar V 0332+53

$E_{cyc,0} \sim 30$ keV $\quad E_{cyc,1} \sim 60$ keV

$P_{spin} \sim 4.4$ sec

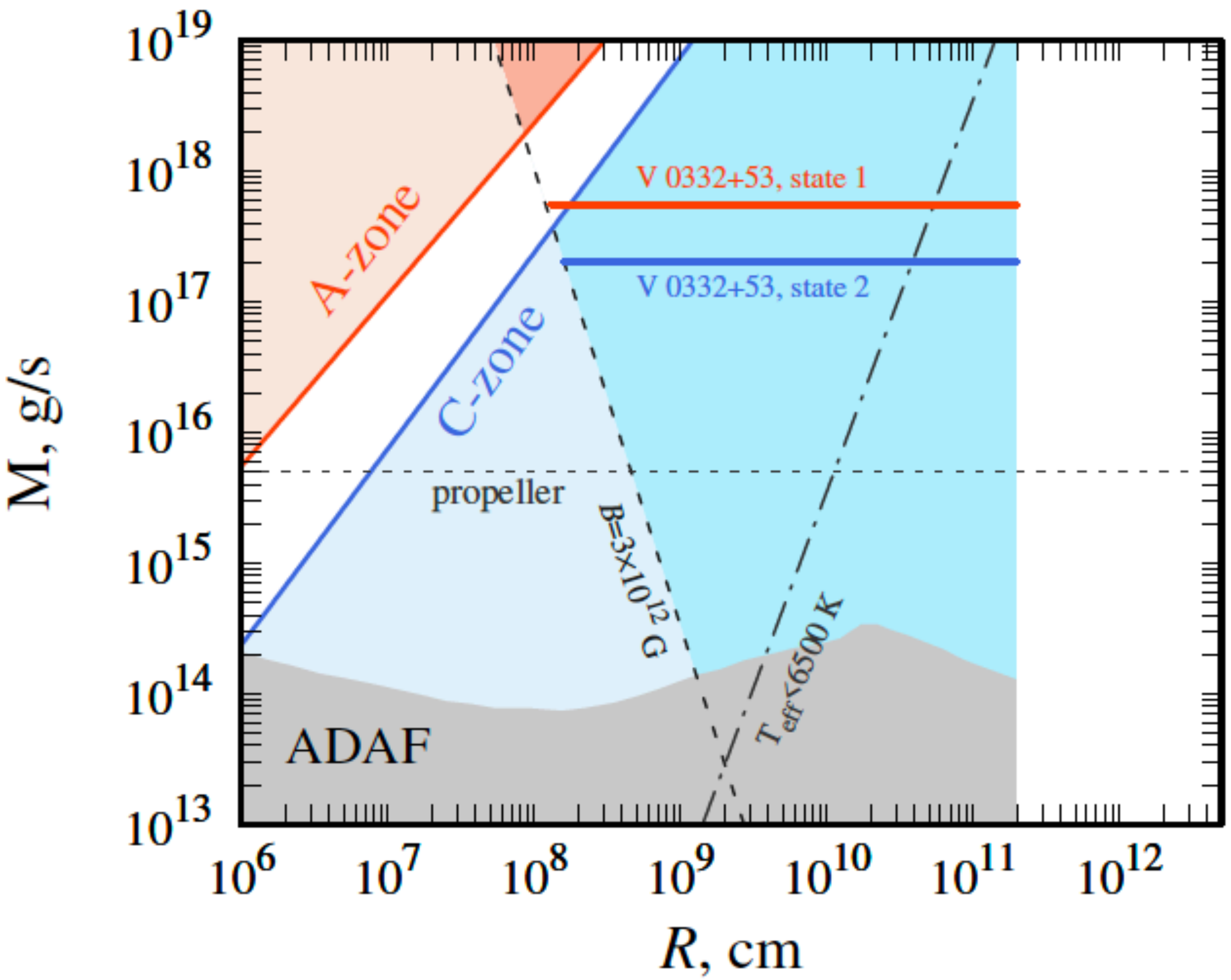

Cooling wave starts at:

$$R_1 = 2.12 \times 10^{10}\, m^{1.88} \dot{M}_{17}^{0.376} \alpha_{-2}^{-0.052}\ \mathrm{cm}$$

Behind the cooling wave, the mass accretion rate drops:

$$\frac{\dot{M}_{\rm cold}}{\dot{M}_{\rm hot}} \approx 0.037 \left(\frac{\alpha_{\rm cold}}{\alpha_{\rm hot}}\right)^{1.16}$$

Cooling wave stops at:

$$R_{\rm out}^{\rm (hot)} \approx 6 \times 10^9\, m^{1.88} \left(\frac{\alpha_{\rm cold}}{\alpha_{\rm hot}}\right)^{0.44} \dot{M}_{17}^{0.376} \alpha_{-2}^{-0.052}\ \mathrm{cm}$$

$R_{\rm out}^{\rm (hot)} \simeq 3.4 \times 10^9$ cm

$R_{\rm out}^{\rm (hot)} = 5 \times 10^9$ cm

Smak, 1984
Cannizzo & Kenyon, 1987

AM+, submitted

X-ray pulsar V 0332+53

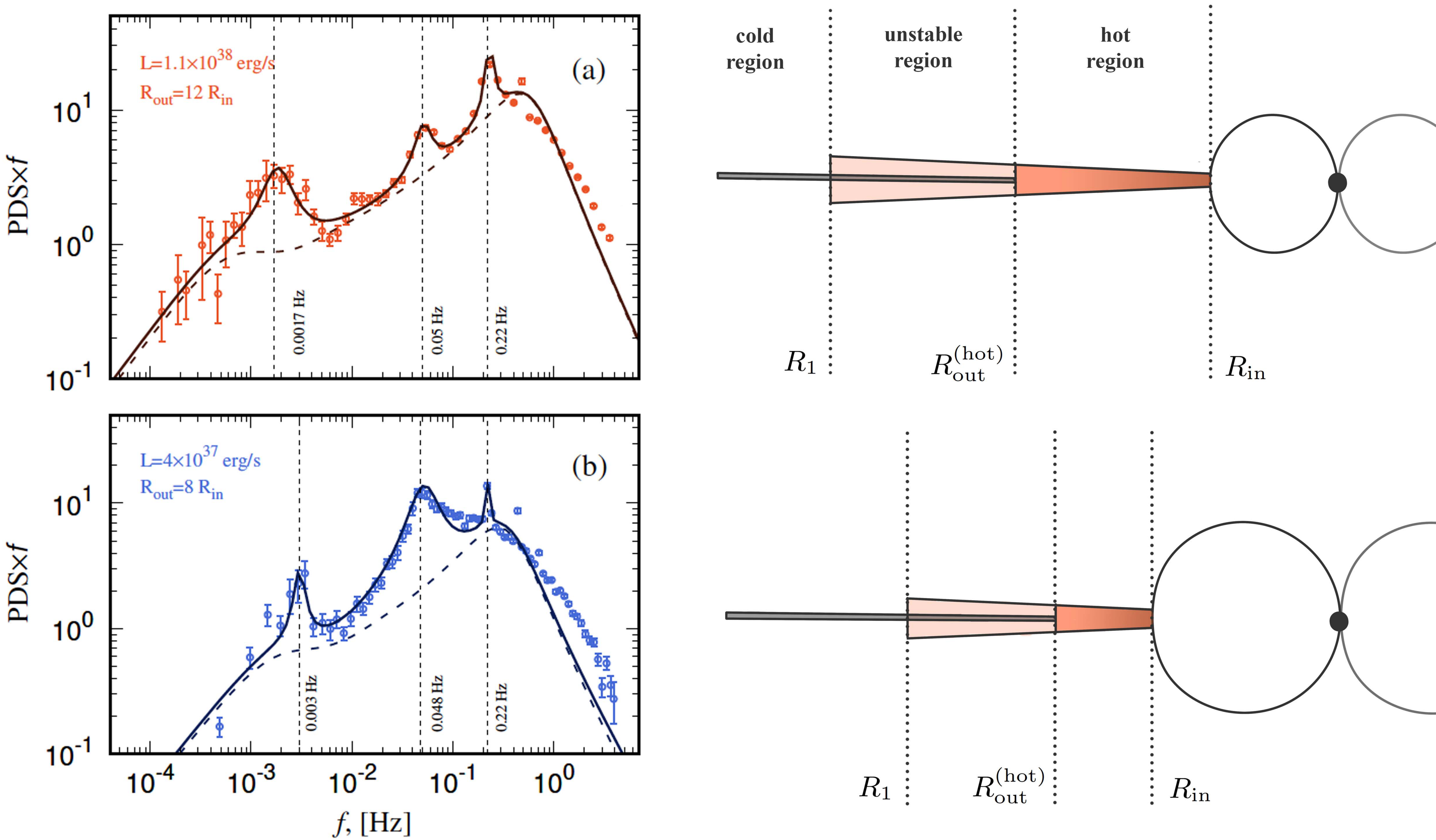

AM+, submitted

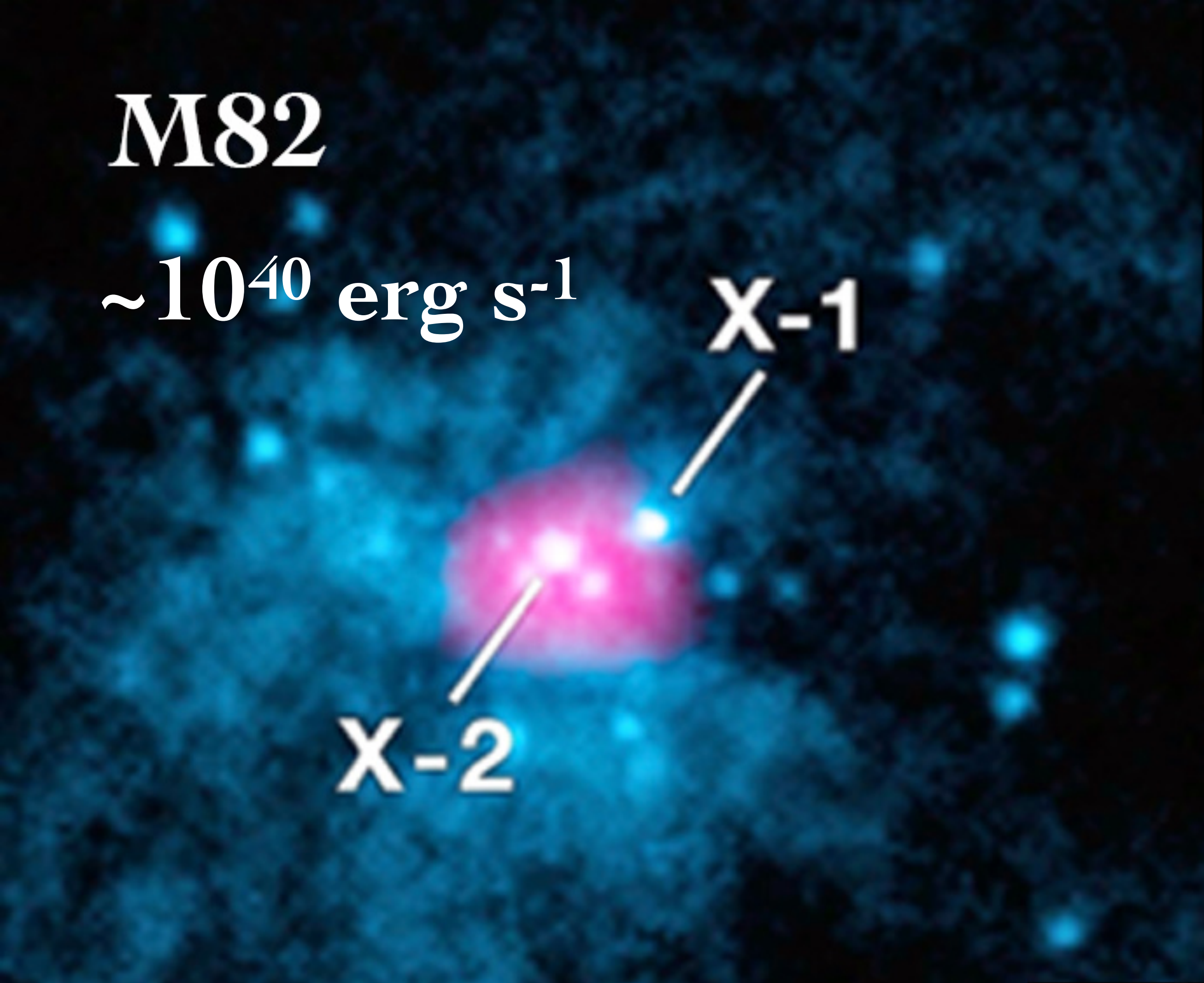
M82
~10^{40} erg s^{-1}
X-1
X-2

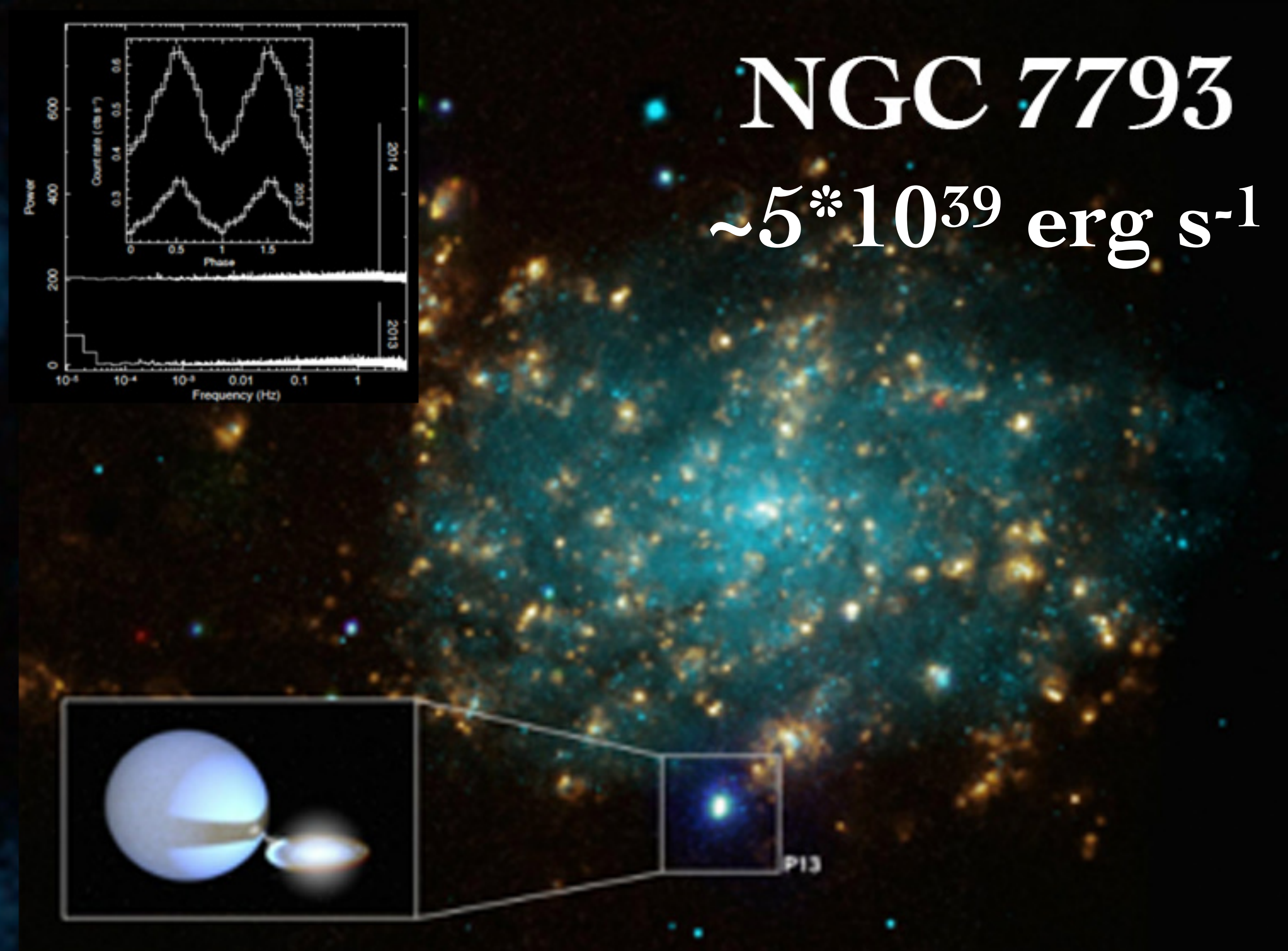
NGC 7793
~$5*10^{39}$ erg s^{-1}
Power
Phase
Frequency (Hz)
2014
2013
P13

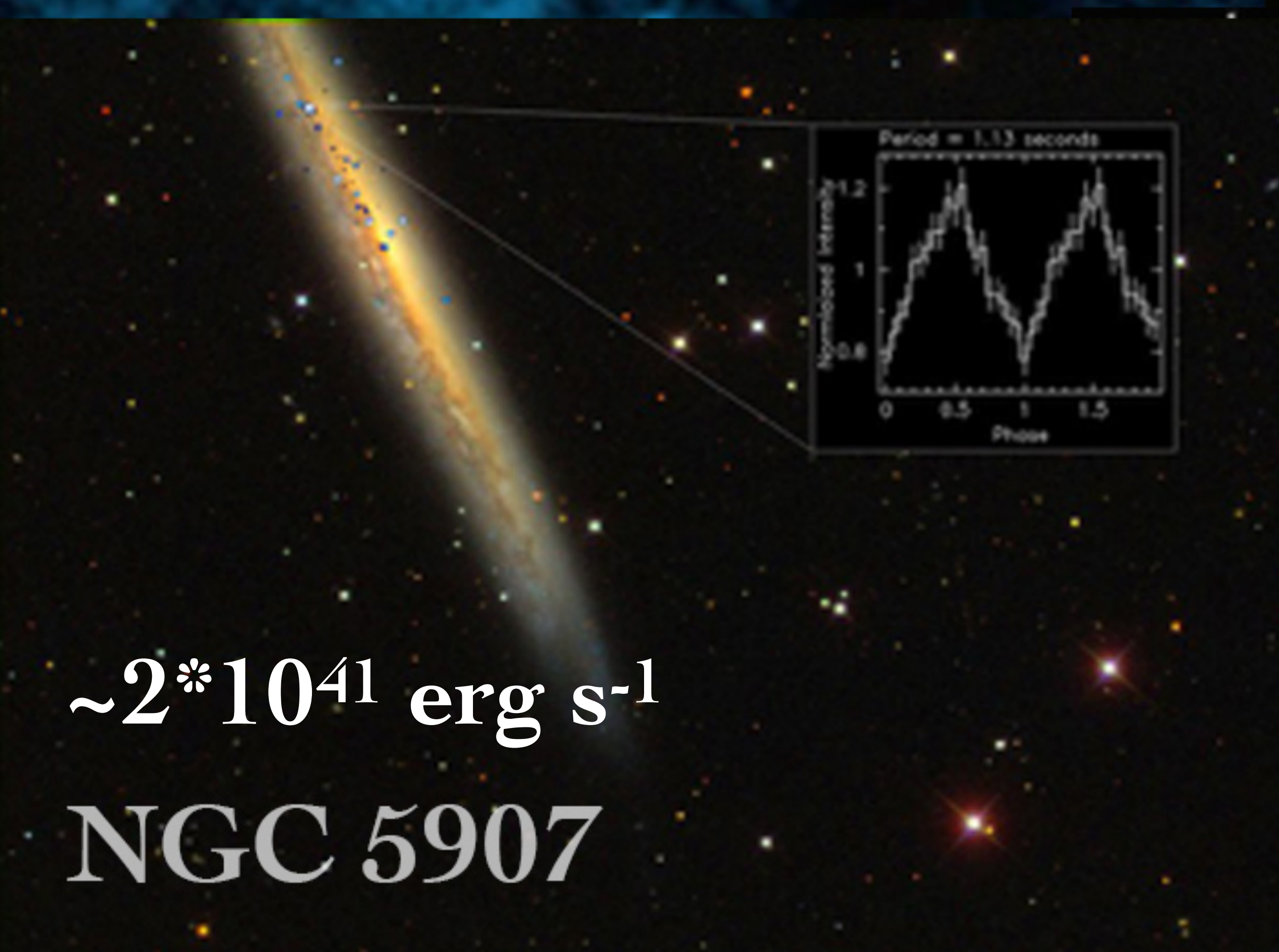
Period = 1.13 seconds
Normalized Intensity
Phase
~$2*10^{41}$ erg s^{-1}
NGC 5907

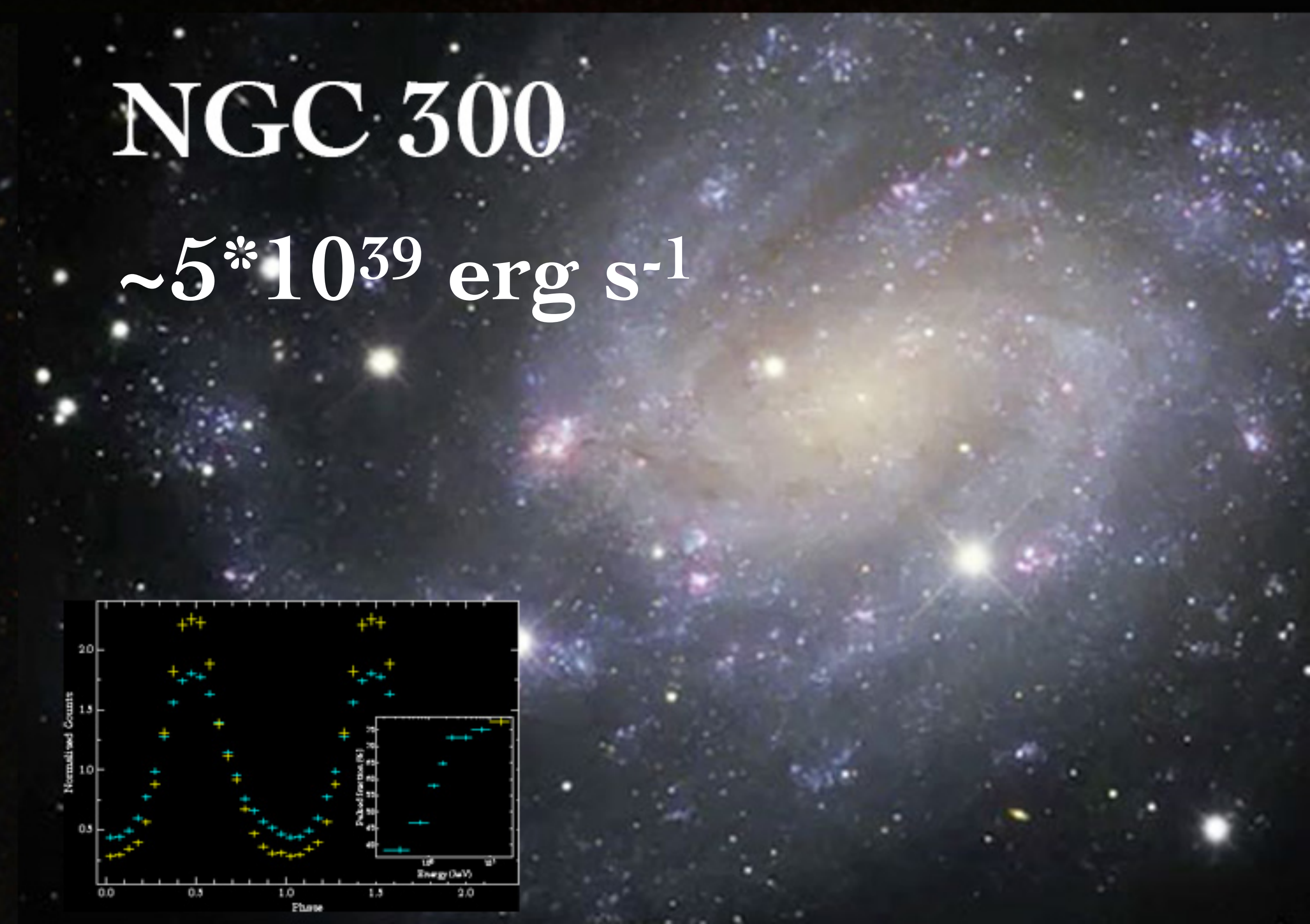
NGC 300
~$5*10^{39}$ erg s^{-1}
Normalized Counts
Phase

Geometrical Beaming vs. Pulsed Fraction

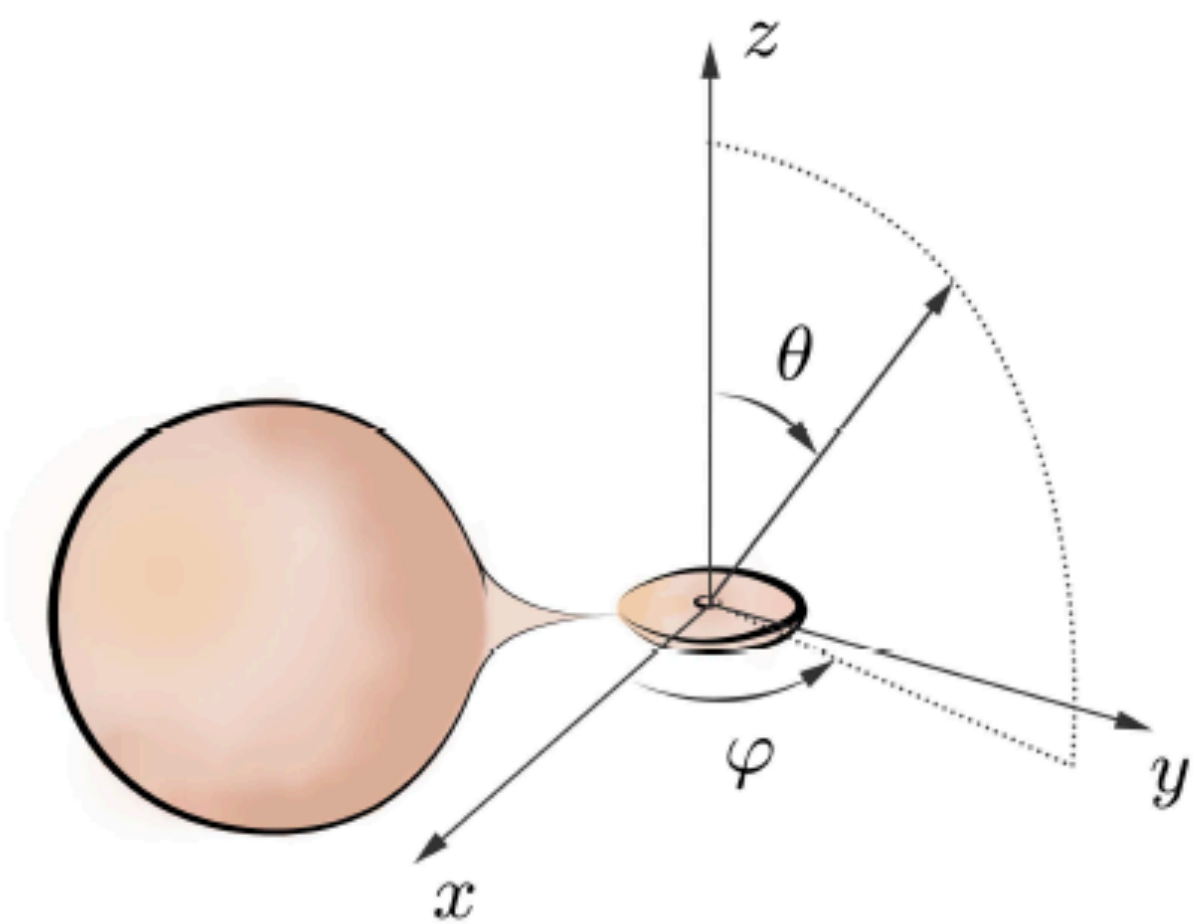

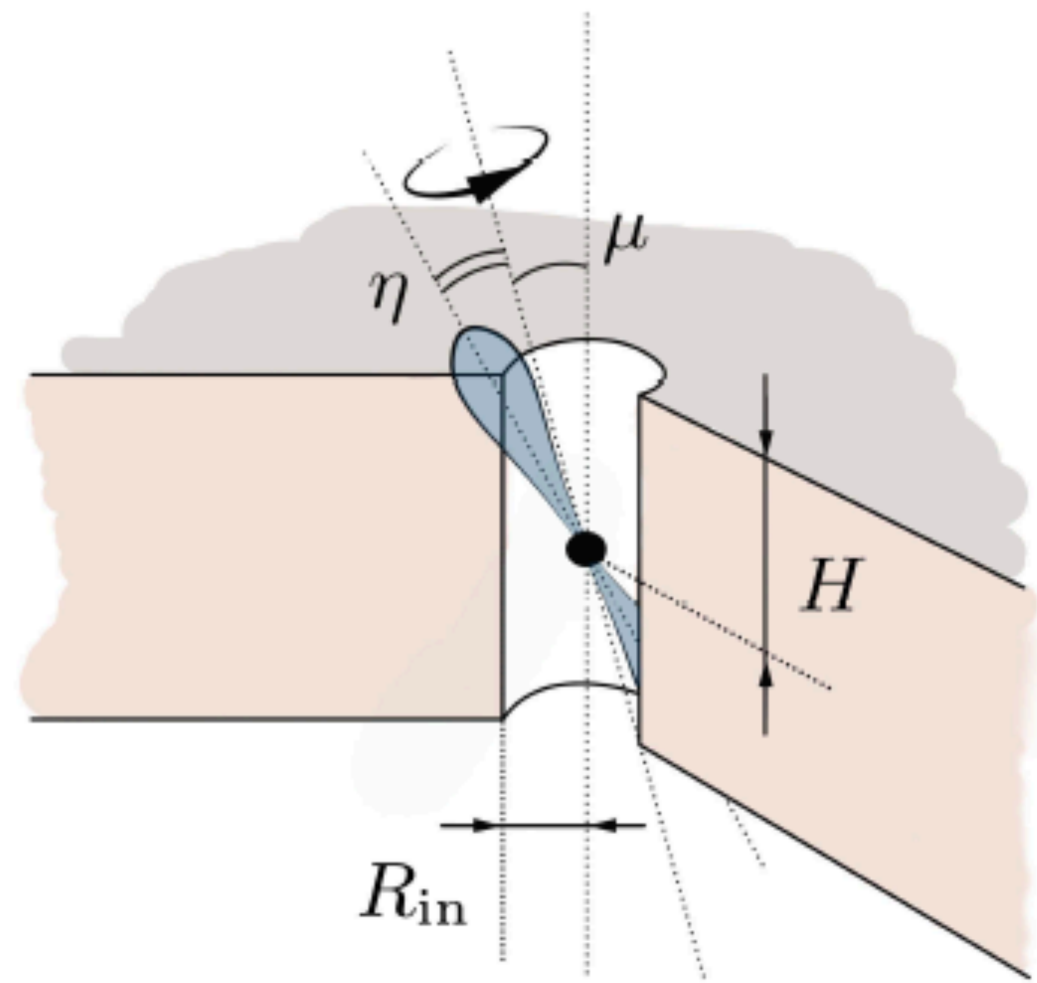

We know **5 pulsating ULXs**.
But, there are only **~15 ULXs** out of **~300** provide the statistics sufficient for detection of pulsations.
(see, e.g., Rodrigues Castillo+, 2020, ApJ, 895)

High Pulsed Fraction (~10 percents and more) is a typical feature of ULX pulsars.

AM+, 2021, MNRAS

No strong beaming in ULX pulsars

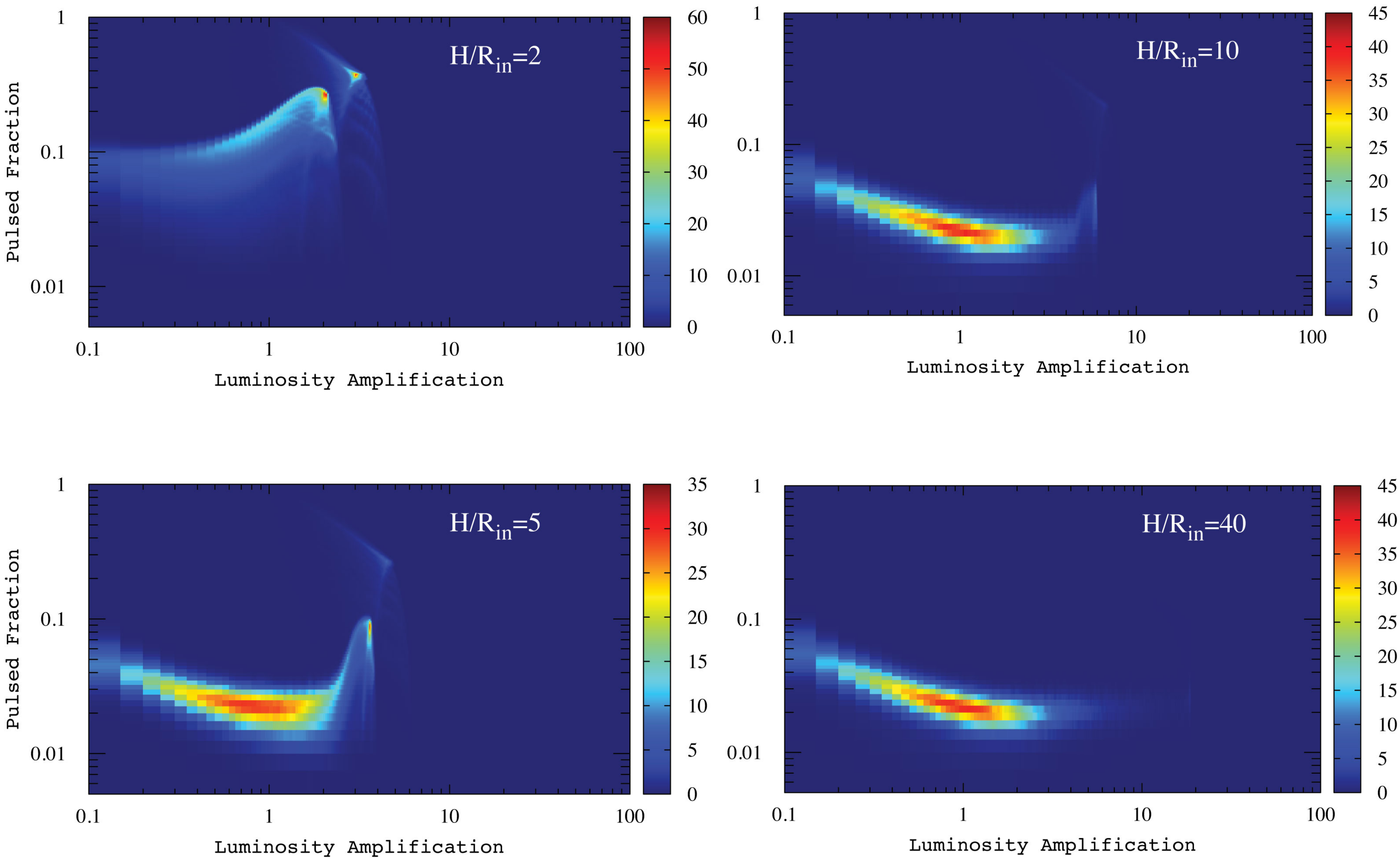

AM+, MNRAS, 2021

Dynamics of the accretion flow in between NS surface and inner disc radius

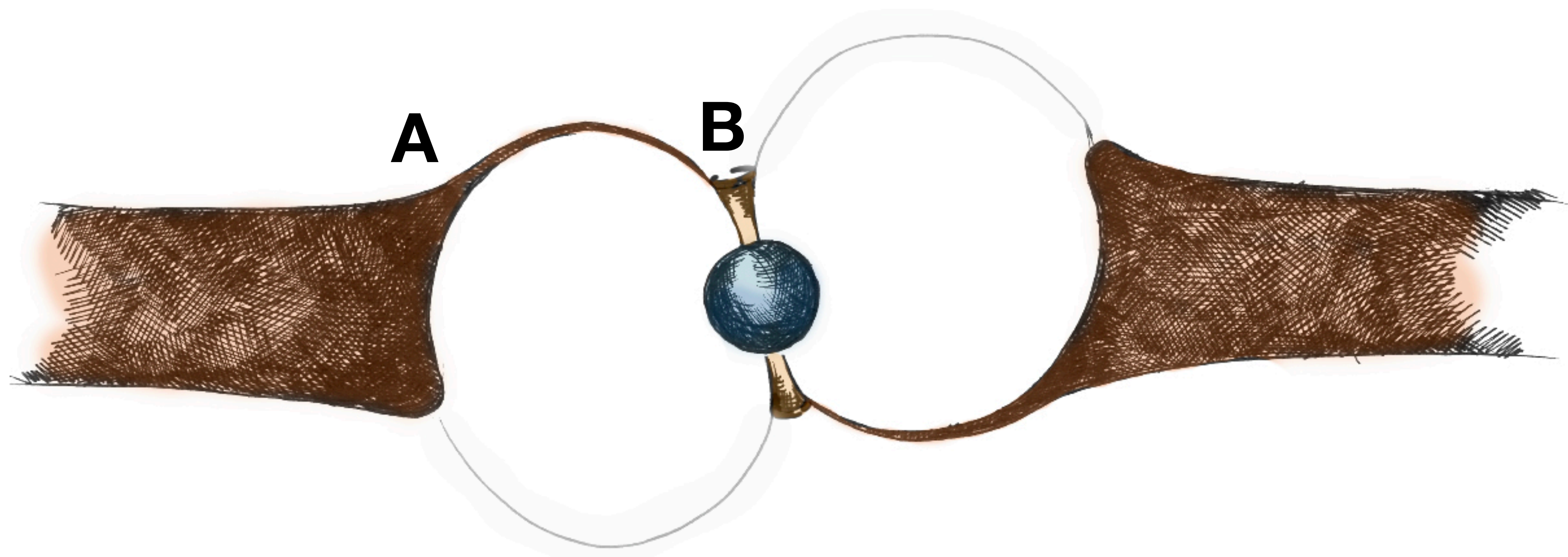

Dynamics of the accretion flow in between NS surface and inner disc radius

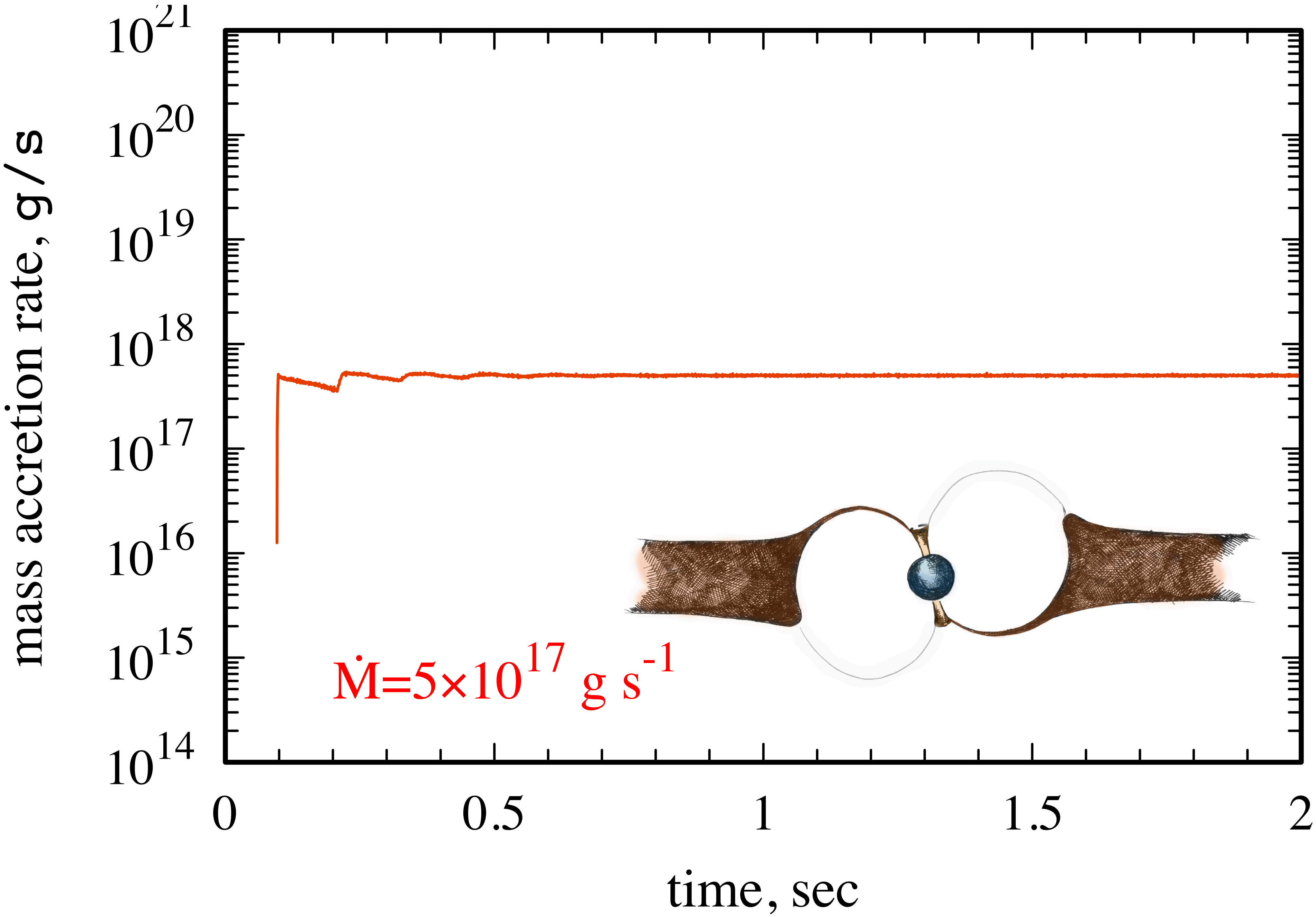

AM+, in prep.

Dynamics of the accretion flow in between NS surface and inner disc radius

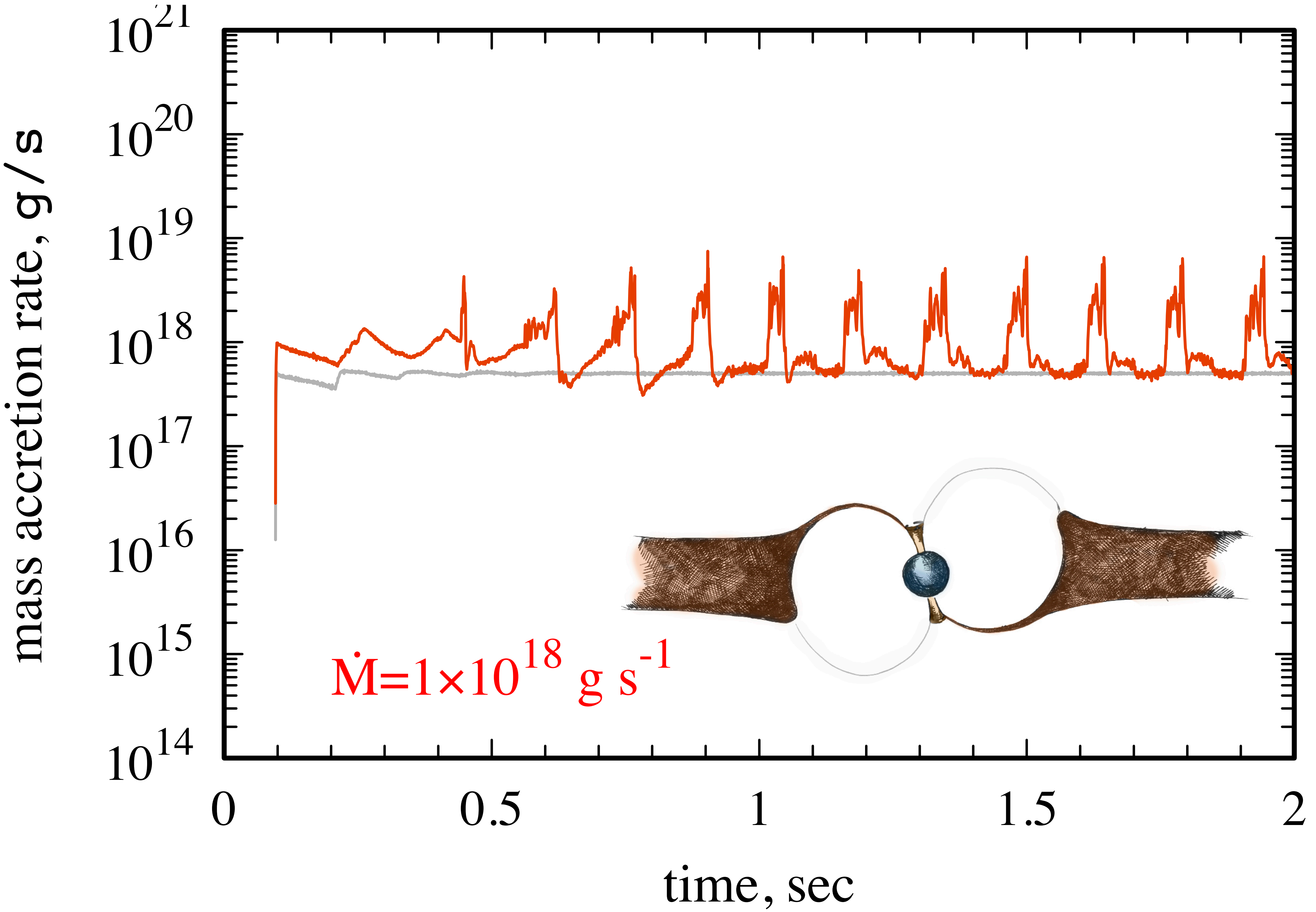

AM+, in prep.

Dynamics of the accretion flow in between NS surface and inner disc radius

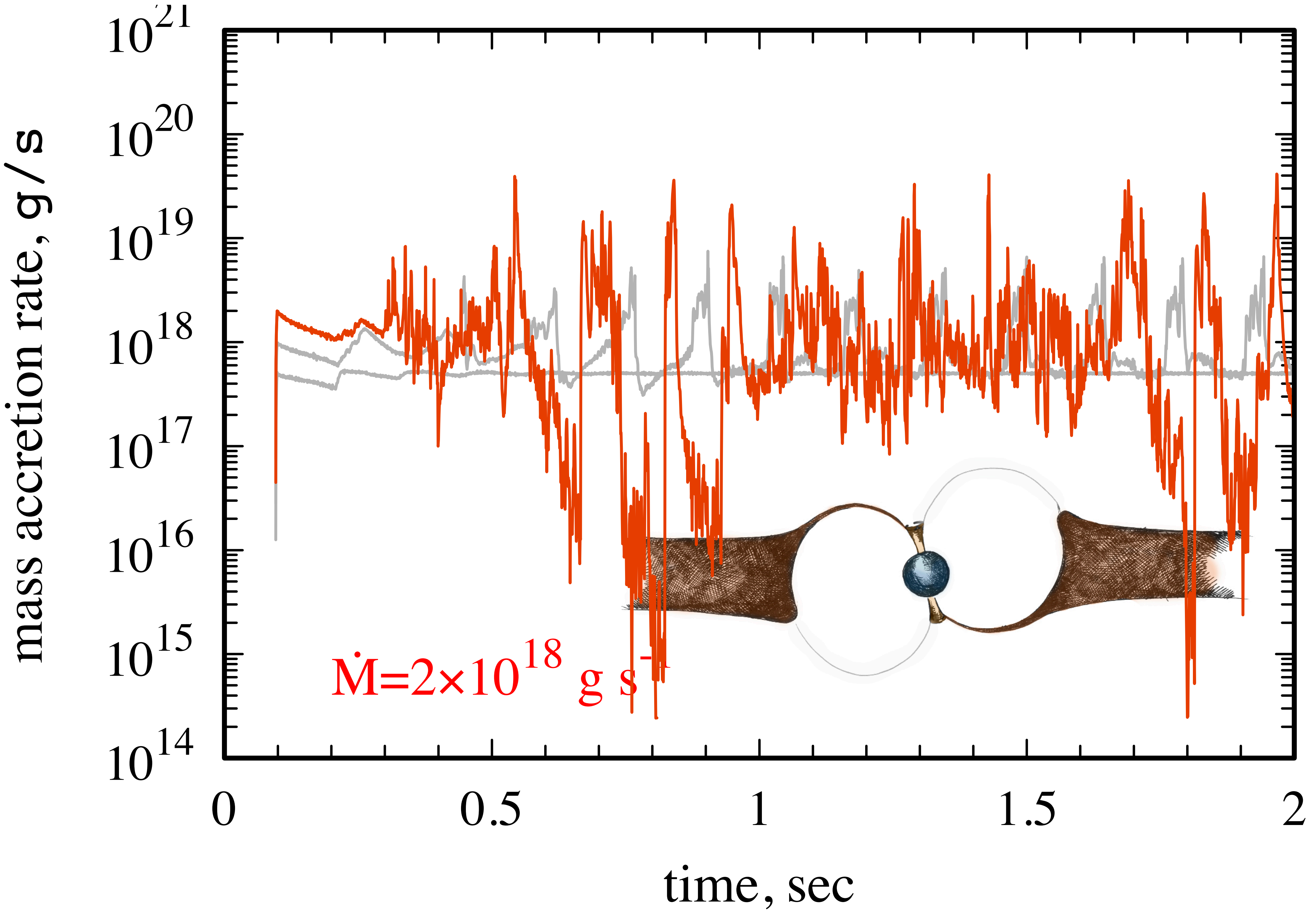

AM+, in prep.

Dynamics of the accretion flow in between NS surface and inner disc radius

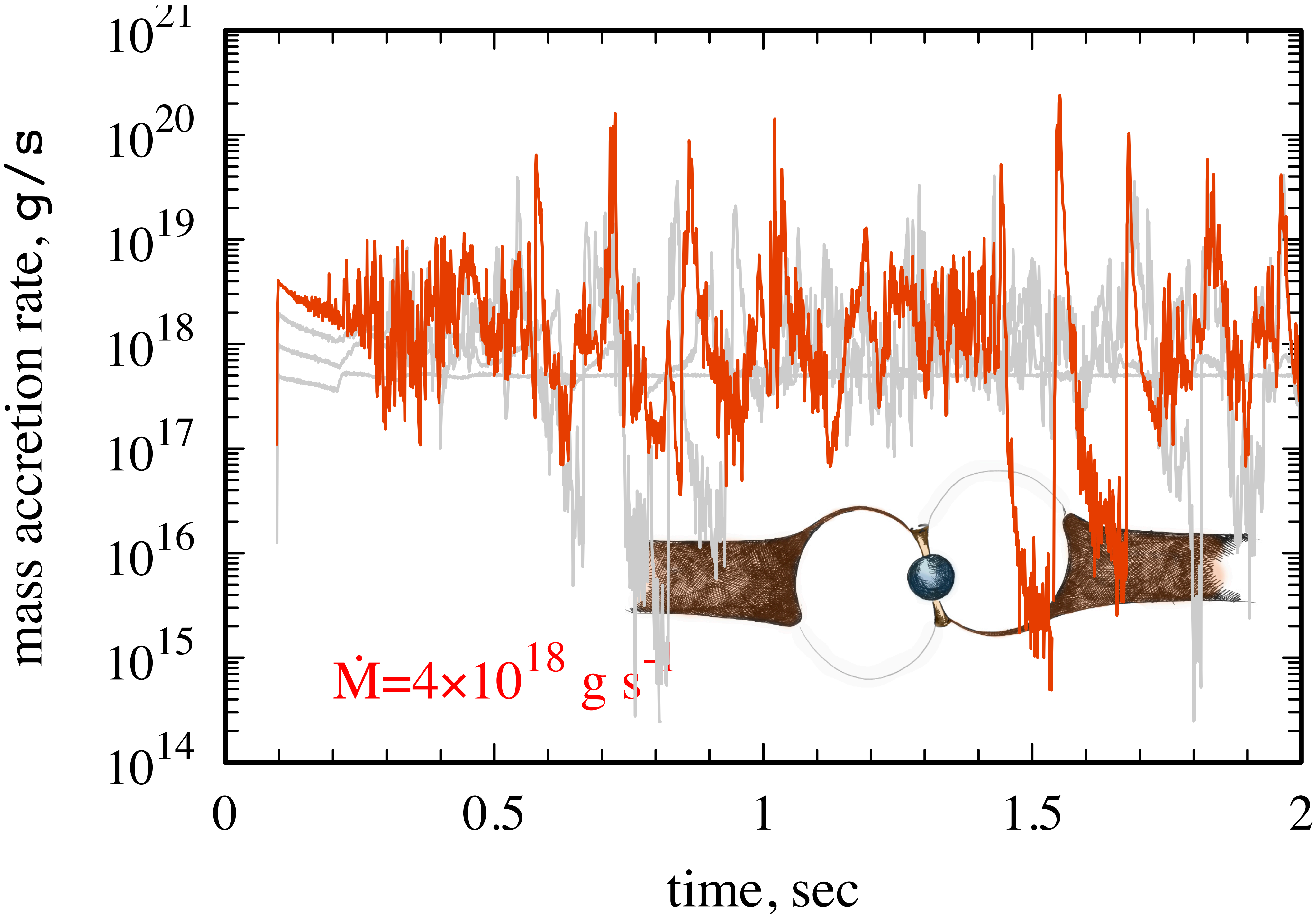

AM+, in prep.

Dynamics of the accretion flow in between NS surface and inner disc radius

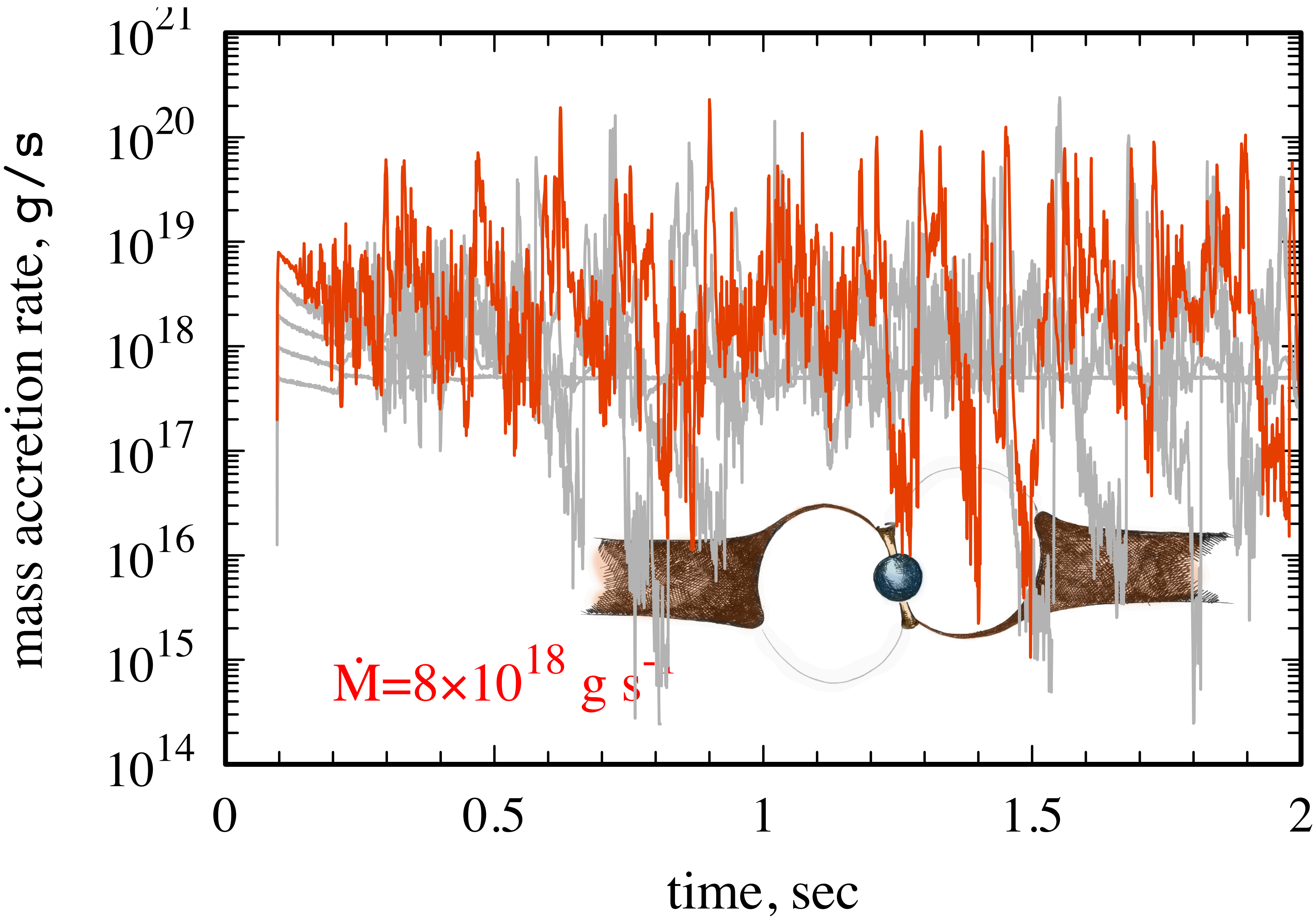

AM+, in prep.

Dynamics of the accretion flow in between NS surface and inner disc radius

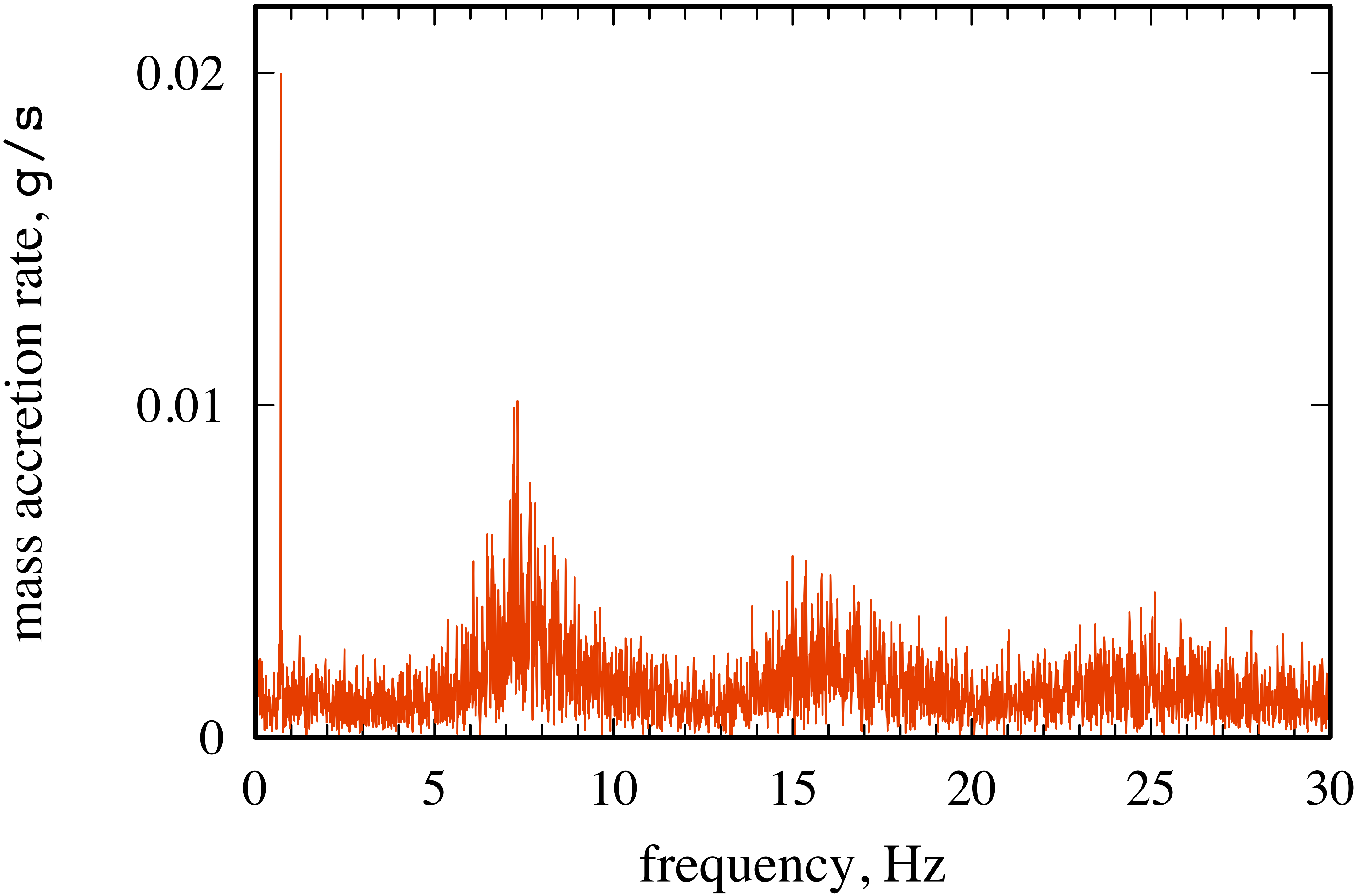

AM+, in prep.

Dynamics of the accretion flow in between NS surface and inner disc radius

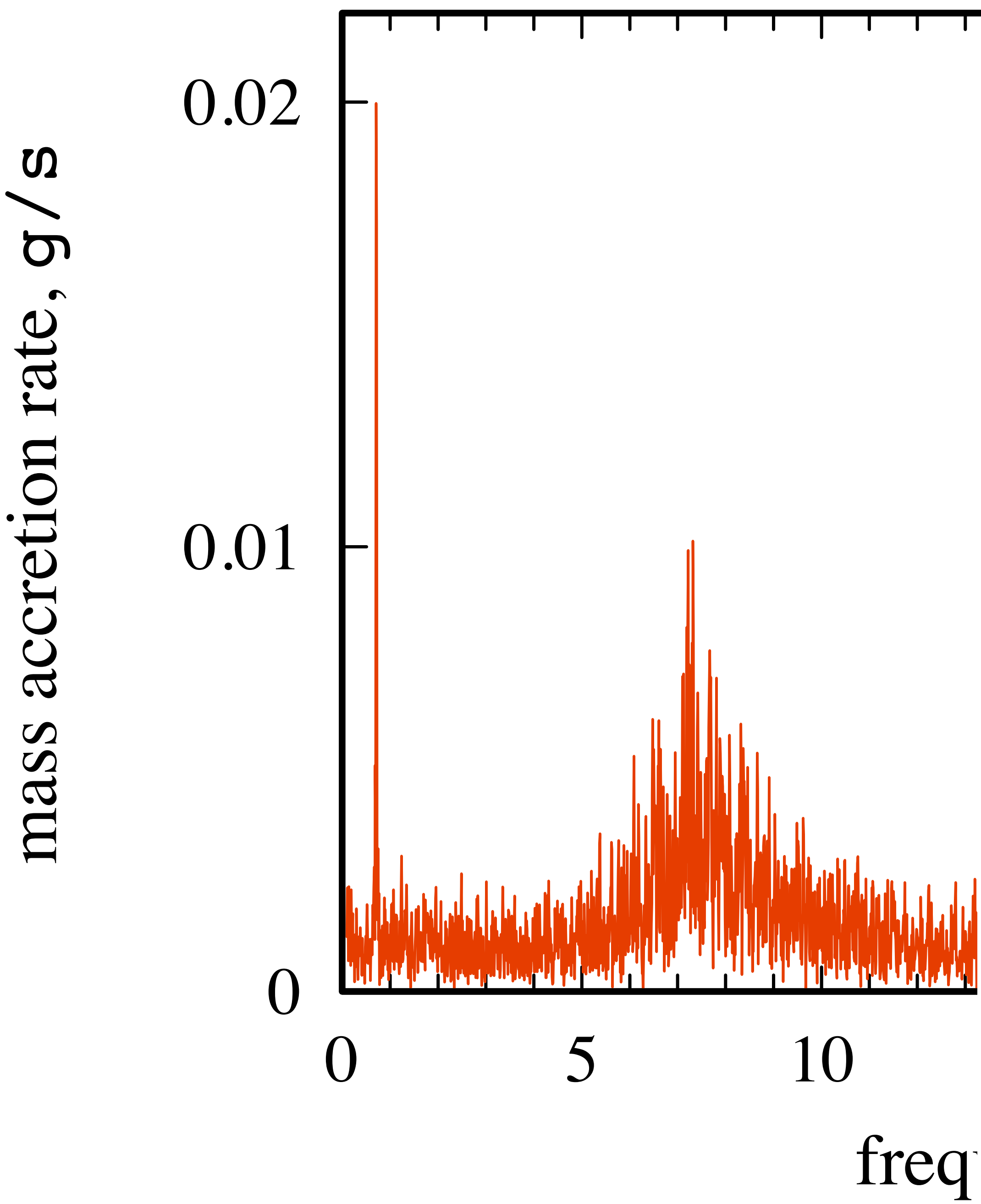

Mönkkönen+, 2019, A&A

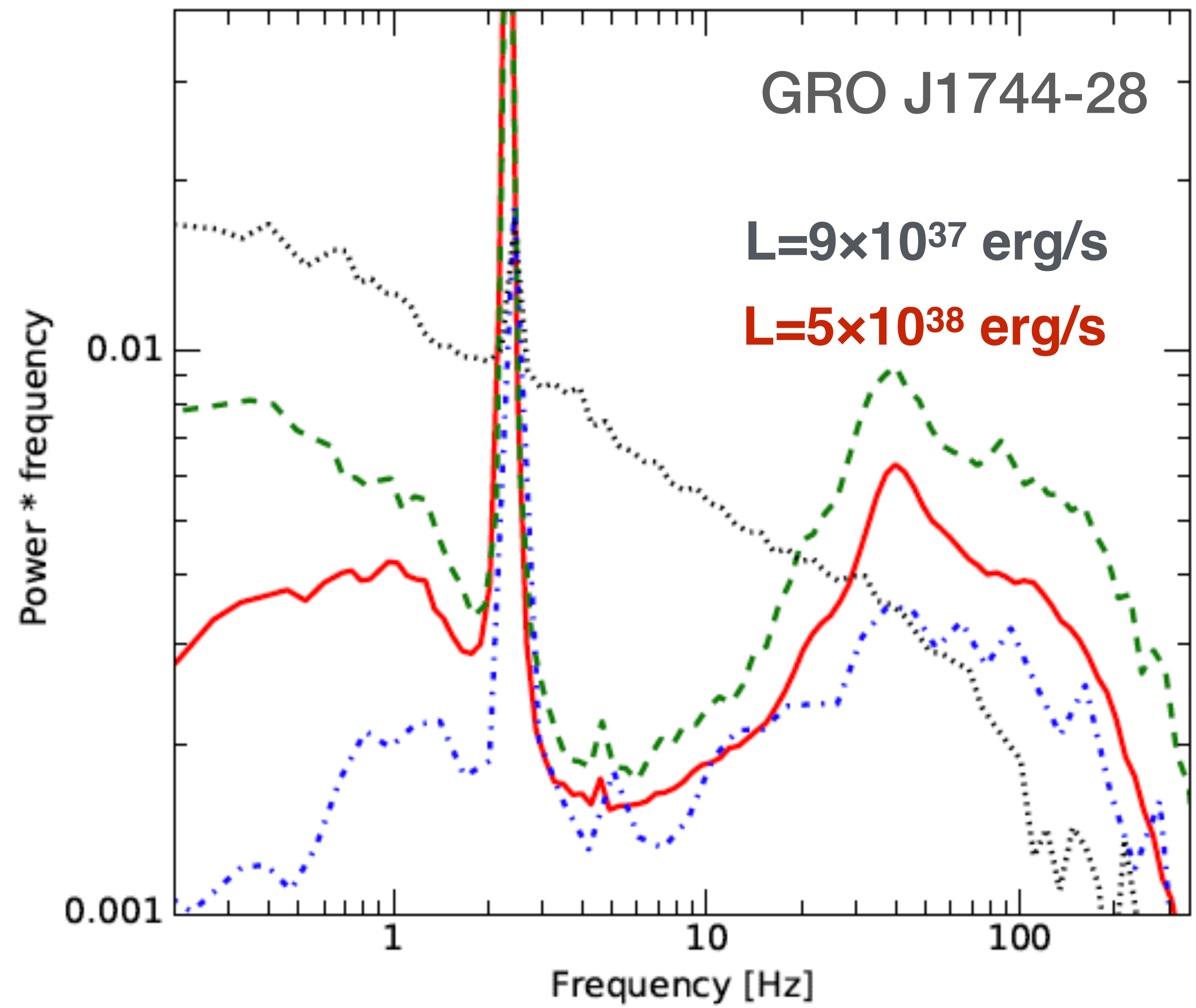

$E_{cyc,0} \sim 4.5$ keV

AM+, in prep.

Conclusions

(a) Broadband PDS of aperiodic variability can be described by the propagating fluctuations model. We do expect **two breaks** in the PDS. **Still, there is an uncertainty in the timing properties of initial fluctuations of viscosity.**

(b) **The high-frequency break** corresponds to the minimal time scale of the dynamo process in a disc. PDS of XRPs can be used as a method of independent measurements of magnetic field strength and structure in XRPs.

(c) **The low-frequency break** corresponds to the viscous time at the outer radius of the hot inner part of the accretion disc.

(d) **Super-Eddington accretion in XRPs results in QPO.** The QPO frequency can used in independent estimations of the inner disc radius and, therefore, magnetic field strength and structure in XRP.